Journal of Hazardous Materials Advances 21 (2026) 101069

Contents lists available at ScienceDirect

Journal of Hazardous Materials Advances

journal homepage: www.elsevier.com/locate/hazadv

Characterization and transcriptome analysis of mercury-resistant *Pseudomonas canadensis* isolated from a chlor-alkali contaminated soil revealed *mer*-independent detoxification pathways

Lorraine Meyer [a], Jun Zhou [b,*], Stéphane Pfendler [b], Siyu Mei [c], Miao Wang [d], Nicolas Capelli [a], Stéphane Guyot [e], Michel Chalot [b]

[a] CNRS, Université Marie et Louis Pasteur, Chrono-environnement (UMR 6249), Besançon F-25000, France
[b] CNRS, Université Marie et Louis Pasteur, Chrono-environnement (UMR 6249), Montbéliard F-25200, France
[c] University of Groningen – GELIFES, Groningen, the Netherlands
[d] Chengdu Academy of Governance, Longquanyi District, Chengdu, Sichuan, China
[e] Université Bourgogne Europe, Institut Agro, INRAE, UMR PAM, Dijon F-21000, France

ARTICLE INFO

Keywords:
Mercury detoxification
Pseudomonas
Stress response
RNA-Seq

ABSTRACT

Human activities have caused severe soil pollution through the discharge of pollutants, reshaping microbial communities. Among soil microbiota, the genus *Pseudomonas* exhibited remarkable tolerance to multiple contaminants, including mercury (Hg). This study compared the Hg resistance mechanisms of two *Pseudomonas canadensis* strains isolated from contrasting environments: a resistant isolate from the rhizosphere of Hg-contaminated soil and a control strain from unpolluted soil. The strain originating from a Hg-enriched soil showed significant biovolatilisation capacity and 20-fold higher Hg resistance compared to the strain isolated from an unpolluted environment. Biomass and necromass responses indicated that the control strain primarily relied on passive resistance, while the resistant strain exhibited active detoxification. Transcriptomic analysis revealed a rapid upregulation of genes associated with metal detoxification and efflux pathways in the resistant strain, independently of the *mer* operon, suggesting alternative resistance mechanisms. In contrast, the control strain exhibited transcriptional signatures of cellular stress, with increased thiol metabolism, DNA repair, and oxidative stress responses. These findings demonstrate that long-term Hg exposure selects for functional adaptations that sustain resistance in microbial populations. This work sheds new lights on Hg tolerance in *P. canadensis* and highlights the potential of naturally adapted strains for bioremediation strategies.

1. Introduction

Mercury (Hg) has been used by humans for centuries in various applications, such as gold mining and chlor-alkali processes, and its industrial use has generated contaminated sediments and effluents containing high concentrations of Hg (Gworek et al., 2020). However, this metal has been ranked third on the Agency for Toxic Substances and Disease Registry's priority list of hazardous substances (ATSDR, 2017), and its widespread dispersion in ecosystems poses a direct threat to the health of living organisms. Indeed, unlike other essential metals, such as iron or zinc, which are necessary for the proper functioning of living organisms, Hg has no biological role (Durand et al., 2015). It does not undergo biotic or abiotic degradation, but can exist in different forms, including methylated forms.

Hg in its elemental form, Hg^0, is highly volatile and, once emitted into the atmosphere, can travel long distances before being redeposited (Meyer et al., 2023). As a result, Hg is widely distributed across the Earth's surface in a variety of ecosystems. Soil is the largest reservoir of Hg on Earth and contains this element in several forms, and biotic processes can impact Hg bioavailability in soils (Gworek et al., 2020; Xu et al., 2014). Some organisms, including soil microbiota, have adapted to cope with Hg toxicity (Meyer et al., 2023). Hg contamination exerts a selection pressure on soil microorganisms, which can lead to restructuring of microbial communities, and some studies have shown that there is a selection of fungal and bacterial strains possessing genes involved in resistance mechanisms (Jia et al., 2022). Hg resistance genes

* Corresponding author.
E-mail address: jun.zhou@univ-fcomte.fr (J. Zhou).

https://doi.org/10.1016/j.hazadv.2026.101069
Received 4 September 2025; Received in revised form 4 February 2026; Accepted 6 February 2026
Available online 9 February 2026

can be located on the main chromosome or carried by plasmids, allowing the acquisition of Hg resistance through horizontal gene transfer (Meyer et al., 2023). Mobile genetic elements are also involved in the evolution of Hg resistance mechanisms and may promote the acquisition of resistance mechanisms following exposure to Hg. In addition, Hg resistance genes tend to be inherited vertically, and although maintaining the *mer* operon has low fitness costs, making it widespread, some *mer* genes are likely to be lost in the absence of selective pressure (Hall et al., 2020).

There are several pathways of resistance to Hg in microorganisms, the mechanisms of which are more or less understood. The *mer* operon represents the most well-characterized bacterial Hg resistance system, comprising genes responsible for Hg transport across cellular compartments and reduction to volatile Hg^0 (Meyer et al., 2023). Biovolatilisation is therefore an important Hg detoxification pathway, particularly in bacteria. However, Hg can also be sequestered outside cells by binding to extracellular polymeric substances containing sulphide groups (Xiang et al., 2022). Furthermore, recent studies have shown that fungal necromass can also efficiently adsorb Hg (Maillard et al., 2022). Finally, Hg can undergo intracellular accumulation by binding to metallothioneins or phytochelatins (Aschner et al., 2006).

Certain bacterial strains belonging to the *Pseudomonas* genus have been isolated on several occasions from environments contaminated with heavy metals (Al-Ansari et al., 2021; Alfarras et al., 2022; Pramanik et al., 2021) and have demonstrated their ability to resist Hg (Bourdineaud et al., 2020; Chang et al., 2021; Pant et al., 2024; Zhang et al., 2020). Despite extensive phenotypic characterisation, transcriptomic investigations of Hg resistance mechanisms in *Pseudomonas* remain limited (Chang et al., 2021; Morales et al., 2021; Zheng et al., 2018). To our knowledge, there are no comparative studies examining strain-specific resistance strategies in the literature. Yet understanding microbial Hg resistance mechanisms is crucial for elucidating the role of microorganisms in global Hg biogeochemical cycling, as well as for identifying potential bioremediation candidates. However, several critical knowledge gaps persist: few studies have examined the gene expression patterns underlying Hg resistance in *Pseudomonas* species, and to date, no studies have compared resistance mechanisms between strains isolated from different environmental contexts. Furthermore, the molecular basis for strain-specific differences in Hg tolerance is not well understood.

This study aims to fill current knowledge gaps by comparing two *Pseudomonas canadensis* strains with contrasting environmental origins. *P. canadensis* has been isolated from diverse habitats—including fertilized agricultural soils, wild mushrooms, and *Zophobas morio* larvae—and is known for its antagonistic activity against fungal and bacterial phytopathogens (Ghasemi et al., 2023; Kundlacz et al., 2024; Mazuecos-Aguilera et al., 2025; Tambong et al., 2016). Its level of resistance to Hg demonstrated by this study further highlights its potential for bioremediation applications, while the availability of genomic data makes it an appropriate model for comparative transcriptomic analyses. In this work, we investigated two strains: *P. canadensis UFC_B020*, isolated from Hg-contaminated rhizospheric soil, and *P. canadensis P31*, from a salt marsh. We hypothesized that their contrasting environmental origins have shaped distinct Hg resistance strategies. To test this, we combined physiological, microscopic, and transcriptomic analyses to characterize and compare the Hg detoxification mechanisms of each strain. Our integrated approach revealed strain-specific molecular responses to Hg exposure and provides the first comparative transcriptomic insight into Hg resistance within the genus *Pseudomonas*, advancing our understanding of microbial adaptation to metal contamination and identifying potential targets for bioremediation.

2. Materials and methods

2.1. Bacterial strains

The *P. canadensis UFC_B020* strain was isolated from a Hg-enriched site located in Saint-Symphorien-sur-Saône in Côte d'Or, France, previously described in other works (Durand et al., 2017). The *P. canadensis P31* strain was kindly provided by the Groningen Institute for Evolutionary Life Sciences (University of Groningen) and was isolated from a Wadden Island salt marsh in the Netherlands, as described in the work of Mei et al. (2023).

2.2. Genome sequencing of UFC_B020

Genomic DNA from *UFC_B020* was extracted from an overnight culture at 30°C and 250 rpm using the E.Z.N.A.® Bacterial DNA kit (Omega Bio-Tek, Inc., Norcross, GA). Extracted DNA was quantified using the Qubit™ dsDNA HS Assay Kit (Invitrogen, Carlsbad, CA, USA) and the A260/A230 and A260/A280 ratios were measured with the Spark® microplate reader (Tecan, Männedorf, Switzerland) to check the quality of the DNA extracts. High-quality DNA was fragmented by mechanical shearing using ultrasonic shearing, followed by purification of the resulting fragments. End repair, 3'-end adenylation, and ligation of sequencing adapters were then performed. Size selection of the ligated fragments was carried out by agarose gel electrophoresis, and the selected fragments were subsequently amplified by PCR to generate the sequencing library. The library was first evaluated for quality, and those passing quality control were sequenced on the Illumina NovaSeq 6000 platform, generating paired-end reads. Raw reads were initially assessed for quality, and low-quality sequences and adapters were filtered using fastp version 0.20.0 (Chen, 2023) to obtain high-quality clean reads. The clean reads were then aligned to the reference genome sequence using BWA version 0.7.17-r1188 (Li et al., 2009). Genomic sequences are available in the NCBI public repository, with the accession number PRJNA1308019.

2.3. Minimal inhibitory concentrations (MIC) of Hg

A Hg stock solution concentrated at 20 mM was prepared by dissolving $HgCl_2$ (Sigma-Aldrich, St-Louis, MO, USA) in ultra-pure water and then diluted as needed for the preparation of culture media. Each strain was pre-cultured in Luria-Bertani (LB) broth (BD, Cockeysville, MD, USA) supplemented with Hg at 30°C under agitation (250 rpm) to reach the stationary growth phase. To determine the MIC of Hg for the two strains, fresh cultures of LB were inoculated by diluting the pre-cultures 100-fold, then supplemented with Hg at different concentrations: 0, 10, 25, 50, 75, 100, 200 and 400 μM. Since strain *P31* did not grow at 10 μM Hg, a lower range of Hg concentrations was tested specifically for this strain: 0.5, 1 and 5 μM. The Hg-supplemented solutions were obtained by diluting the Hg stock solution in LB medium. After 48 h of incubation at 30°C under agitation (250 rpm), the Optical Density at 600 nm (OD_{600}) of the cultures was measured to assess bacterial growth. For each concentration tested, the OD_{600} was measured in triplicate from three independent cultures.

2.4. Growth kinetics

Each strain was pre-cultured in LB broth supplemented with Hg at 30°C under agitation (250 rpm) to reach the stationary growth phase. Fresh cultures of LB were inoculated by diluting the pre-cultures 100-fold, then incubated at 30°C under agitation (250 rpm). For each strain, three independent cultures were grown in LB broth only or enriched with Hg (at concentrations of 20 μM for *UFC_B020* and 1 μM for *P31*, respectively, corresponding to 10% of the MIC). At the beginning of the incubation and every hour for a total duration of 10 h, the OD_{600} of the cultures was measured to assess bacterial growth. Kinetic parameters

(growth rate, generation time, lag time) were estimated with the Sym'previus software (https://symprevius.eu/en/, accessed on 28/10/2024) from experimental growth kinetics data using the primary growth model (Le Marc & Coroller, 2025).

2.5. Bacterial cultures for Hg monitoring and RNA extraction

Each strain was pre-cultured in LB broth supplemented with Hg at 30°C under agitation (250 rpm). Fresh cultures of LB broth were inoculated by diluting the pre-cultures 100-fold, then incubated at 30°C under agitation (250 rpm) until the OD_{600} reached 0.4-0.5, corresponding to the start of the exponential phase (LaVoie & Summers, 2018). Hg was then added to the medium for further incubation. Two Hg concentrations were tested: 0 μM, and 20 μM for *UFC_B020* or 1 μM for *P31*. These concentrations correspond to 10% of their respective Hg MIC values. Two exposure times were tested: 30 min (t1, approximately one generation cycle, for short-term effects on bacteria) and 3 h (t2, after more than three cell divisions, for long-term effects). Immediately after the Hg was added and the culture medium homogenised, aliquots of cultures were collected to measure the initial Hg concentration in the medium.

At the end of the exposition times, the OD_{600} of the cultures was measured and the cells were recovered by centrifugation for 5 min at 4°C and 14,000 x *g*. They were washed in PBS (Sigma-Adrich, St-Louis, MO, USA) and then centrifuged again for 5 min at 4°C and 14,000 x *g*. The bacterial pellets were immediately frozen at -80°C until RNA extractions. For each condition, additional aliquots of cultures were collected and pooled for Hg measurements: samples were centrifuged for 5 min at 14,000 x *g*, the supernatants were recovered, and the pellets were washed 3 times in PBS before being finally resuspended in an equivalent volume of PBS. Hg measurements were performed with the AMA 254 (Altec Ltd., Prague, Czech Republic) according to the following steps and their respective parameters: a first phase of 35 s for sample drying, a second phase of 150 s for sample decomposition and a final phase of 45 s for Hg release and quantification by atomic absorption spectrometry at a wavelength of 245 nm. Tobacco leaves (Oriental Basma Tobacco Leaves, INCT-OBTL-5, ICHTJ, Poland) were used as certified reference material. For each condition and for each strain, Hg measurements were performed in three biological replicates, and each Hg quantification was performed from a pool of three independent bacterial cultures. Control solutions containing Hg (at concentrations of 20 μM and 1 μM) but no bacterial material were incubated in the same conditions in triplicates to evaluate spontaneous Hg volatilisation at 30°C.

2.6. Bacterial necromass incubation with Hg

Each strain was pre-cultured in LB broth supplemented with Hg at 30°C under agitation (250 rpm). Fresh cultures of LB broth were grown as previously described until the OD_{600} reached 0.4-0.5. Chloramphenicol (Euromedex, Souffelweyersheim, France) was added at a final concentration of 1 g/L in each bacterial culture. The cultures were incubated again for 24 h at 30°C under agitation (250 rpm). After incubation with chloramphenicol to obtain bacterial necromass, Hg was added to the medium and the same protocol described in the previous section was followed for the monitoring of Hg concentration with bacterial necromass. The bacterial necromass solution obtained after incubation with chloramphenicol was inoculated onto LB agar medium and then incubated at 30°C for 24 h to check that there was no growth and that the bacteria were indeed dead.

2.7. Hg material balance

After Hg quantification with the AMA 254, several parameters were calculated to reconstruct the various passive and active transfers of Hg within the biomass and bacterial necromass (Chang et al., 2021; Chen et al., 2018b). Each parameter and its associated equation are described below:

- The Hg remaining rate which corresponds to the percentage of Hg remaining in the culture medium after incubation.

$$k_{remain} = \frac{C_{medium} \times 100}{C_0} \quad (1)$$

With C_{medium}, the Hg concentration in the culture medium after incubation and C_0, the initial Hg concentration.

- The Hg bacterial rate which corresponds to the percentage of Hg measured in the bacterial material after incubation.

$$k_{bact} = \frac{C_{bact} \times 100}{C_0} \quad (2)$$

With C_{bact}, the Hg concentration in the resuspended bacterial pellet after incubation and C_0, the initial Hg concentration.

2.8. Microscopic observations with Hg-specific fluorescent probes

4-(2-aminophenyl)-7-(diethylamino)-3-(1,3-dithiolan-2-yl)-3-formylcoumarin (ATC-Hg) is an exogenous probe which enables the detection of both Hg^{2+} and MeHg. This molecule was synthesised as described in Pan et al. (2018) by the synthesis platform of the Institut de Chimie et Biochimie Moléculaires et Supramoléculaires (Lyon, France), with a final purity of 95%. A stock solution of ATC-Hg concentrated at 5 mM was prepared in DiMethyl SulfOxide (DMSO) and stored at -20°C. Briefly, ATC-Hg fluorescence relies on the ortho 2-aminophenyl group installed to the Hg^{2+}/MeHg-reactive 1,3-dithiolane moiety, which causes the fluorescence change of coumarin derivatives through an intramolecular charge transfer. The final product of the reaction is a heterocyclic aromatic compound whose fluorescent signal enables bacterial imaging.

The two strains *UFC_B020* and *P31* were pre-cultured in LB broth at 30°C under agitation (250 rpm) to reach the stationary growth phase. Fresh bacterial cultures were centrifuged at 4000 x *g* for 3 min and bacterial pellets were washed three times in PBS. Bacterial pellets were then resuspended in PBS and divided into two groups: the control group and the experimental group. The control group was incubated with 5 μM ATC-Hg for 5 min at 30°C and then washed 3 times with PBS. The experimental group was treated in the same way as the control group and was then incubated at different concentrations of Hg (10, 20 and 100 μM) for 5 min at 30°C. Contrary to what is described in Pan et al. (2018), the bacteria were first incubated with the probe and then with Hg, in order to limit potential biovolatilisation. Bacteria from the 2 groups were then observed directly in PBS with a two-photon microscope. A second incubation protocol was tested at 20 μM Hg: the bacteria were incubated with the ATC-Hg probe first and then with Hg for 30 min before being observed under a two-photon microscope.

Two-photon imaging microscopy was performed on a Nikon A1-MP scanning microscope equipped with a Plan APO IR × 60 objective (NA, 1.27; Water Immersion, Nikon). An IR laser (Chameleon, Coherent) was used to provide excitation at 810 nm. Fluorescence emission was collected on two detection channels: FF03-525/50 (500–550 nm) and FF01-629/56 (601–657 nm) (Semrock). All images were processed in the same way. The obtained images were analysed using ImageJ software (version 1.54p), with Java version 1.8.0_322 (Schindelin et al., 2012). First, ratio images of the red/green channels were obtained using the RatioPlus plugin. Threshold correction using the Otsu method was then performed on each ratio image to distinguish the cells from the background, and the intensity was measured in the area delimited by

Otsu thresholding. For each condition, a minimum of three images was analysed.

2.9. RNA extraction, library preparation and sequencing

Bacterial pellets were slowly thawed on ice and RNA extractions were performed using the RNeasy Mini Kit (Qiagen, Hilden, Germany) following the manufacturer's instructions, including the optional DNase step. RNA quality and quantity were assessed with the Nanodrop (ThermoFisher Scientific, Waltham, MA, USA) and by running extracts on agarose gel. RNA extracts were stored at -80°C until sequencing. For each condition and for each strain, RNA extractions were performed in three biological replicates, and each extraction was performed from a pool of three independent bacterial cultures.

Library construction and Illumina sequencing were performed by Novogene (Cambridge, UK). Raw reads were processed with fastp software to remove reads containing adapters, reads containing poly-N, and low-quality reads (Chen et al., 2018a) and the Q20, Q30 and GC content were calculated. Clean reads were then aligned on the genome sequence of *Pseudomonas canadensis* PseudoSSchier:P31 (Mei et al., 2023) with Bowtie2 v2.2.3 (Langmead & Salzberg, 2012). Rockhopper was used to identify novel genes. HTSeq v0.6.1 was used to count the read numbers mapped to each gene and the expected number of Fragments Per Kilobase of transcript sequence per Millions base pair-sequenced (FPKM) of each gene was calculated based on the length of the gene and read count mapped to this gene (Anders et al., 2014). RNA sequence data are available in the NCBI public repository, with the accession number PRJNA1277159.

2.10. Gene expression analysis

K-means clustering was performed from read count data using the iDEP 2.01 webtool (integrated Differential Expression and Pathway analysis, https://bioinformatics.sdstate.edu/idep/, accessed on 09/04/2025) (Ge et al., 2018). The top 400 genes with the lowest standard deviation for their expression levels were considered for clustering, and the number of clusters was determined following the elbow method. For each cluster, networks of enriched Gene Ontology (GO) terms related to Biological Process (BP) were generated with iDEP 2.01. The fold-change of transcripts and the screening of Differentially Expressed Genes (DEGs) were performed with DESeq2 version 42.1 using the R package Bioconductor (Love et al., 2014). The criteria for significant difference expression were set to $|\log_2\text{FoldChange}| > 1.5$ and false discovery rate (FDR) < 0.05, with $\log_2$FoldChange corresponding to the $\log_2$ of the expression ratio of a gene between a test condition and a defined control condition and FDR corresponding to the p-value adjusted with the Benjamini-Hochberg correction. GO enrichment analysis was implemented by the GOseq R package, in which gene length bias was corrected. GO terms with corrected p-values < 0.05 were considered significantly enriched by DEGs. In addition, all DEGs were mapped to terms in the Kyoto Encyclopedia of Genes and Genomes (KEGG) database to identify the enriched KEGG terms (Kanehisa, 2000). Venn diagrams were generated with the VennDiagram R package; other plots were generated with the ggplot2 R package. DEGs were grouped together by biological role within the cells according to associated GO terms and main functions based on literature searches and descriptions from UniProtKB (Bateman et al., 2022).

To investigate Hg resistance determinants, sequencing reads were first aligned to reference *mer* gene sequences using Bowtie2 version 2.3.5.1 (Langmead & Salzberg, 2012) with default parameters. Aligned reads were then assembled *de novo* with SPAdes version 2.15.4 (Prjibelski et al., 2020) to reconstruct potential *mer* operon fragments. Candidate *mer* genes were identified based on homology searches against the NCBI non-redundant protein database. For expression analysis, RNA-seq reads obtained under control and Hg stress conditions were mapped to the predicted *mer* gene sequences using Bowtie2 version 2.3.5.1.

2.11. Statistical analysis

The results were analysed with the software RStudio version 4.3.1. As the normal distribution of the data was not confirmed, non-parametric Kruskal-Wallis tests were carried out to compare the different conditions of a given experiment, and if the p-value was less than 0.05, the post-hoc Dunn's test was performed to form the groups according to their significance. The FactoMineR package in R was used to perform Principal Component Analysis (PCA).

3. Results

3.1. Characterization of bacterial growth under Hg stress

The level of Hg resistance for *P31* and *UFC_B020* strains was assessed by culturing them in a medium with increasing concentrations of Hg. The MIC, defined as the lowest Hg concentration inhibiting growth, was 10 μM for *P31* and 200 μM for *UFC_B020*. Therefore, *UFC_B020* was 20 times more resistant to Hg compared to *P31* (Fig. 1**A**). The growth of bacteria over time, both with and without Hg stress, was also characterised. A Hg concentration corresponding to 10% of the MIC was set, *i.e.* 20 μM for *UFC_B020* and 1 μM for *P31*. The growth curves (Fig. 1**B**) showed that *UFC_B020* grew faster overall. The growth kinetics parameters calculated in Table 1 showed that the growth rate of *UFC_B020* was higher than that of *P31*, whether in the presence of Hg or not. The generation time was approximately 27 min for *UFC_B020* and more than 45 min for *P31*, whatever the condition. Under Hg stress, the lag time of *P31* increased, indicating that Hg had deleterious effects on cell machinery.

3.2. Quantification of Hg in the presence of bacterial biomass versus necromass

The concentration of Hg was measured in both the culture medium and the bacterial material to investigate potential resistance pathways for coping with Hg toxicity. Moreover, both bacterial biomass and necromass were incubated under the same conditions for *UFC_B020* and *P31* to compare passive and active mechanisms (Fig. 2). Regarding *UFC_B020* biomass, significant Hg removal occurred within 30 min of incubation, with less than 25% of the initial Hg concentration remaining in the medium after 3 h. In contrast, no significant differences were observed between *UFC_B020* necromass and the 20 μM Hg control after either 30 min or 3 h of incubation (Fig. 2**A**). Hg resistance and removal were therefore related to active Hg biovolatilisation processes in the *UFC_B020* strain. Strain *P31* exhibited a significant decrease in Hg concentration in the medium for both biomass and necromass compared with the 1 μM Hg control. After 3 h of incubation, the remaining Hg rate k_{remain} for biomass and necromass was roughly equivalent, suggesting that only passive Hg transfer mechanisms were involved in *P31*. These results are consistent with those observed for the Hg bacterial rate k_{bact} in *P31* (Fig. 2**B**). Indeed, some of the Hg present in the medium was probably adsorbed by both the biomass and the necromass of *P31*, which could explain the Hg removal capacity observed previously.

3.3. In vivo imaging with a Hg-specific exogenous fluorescent probe

Observations of bacteria using a two-photon microscope after incubation first with the ATC-Hg probe and then with different concentrations of Hg are shown in Fig. 3. The ATC-Hg probe, synthesized via the covalent assembly principle, emits fluorescence specifically upon Hg binding and has already demonstrated its effectiveness for *in vivo* imaging with *Escherichia coli* (Pan et al., 2018): this exogenous probe was therefore used to compare the behaviour of strains *UFC_B020* and *P31* in relation to Hg exposure via microscopic imaging.

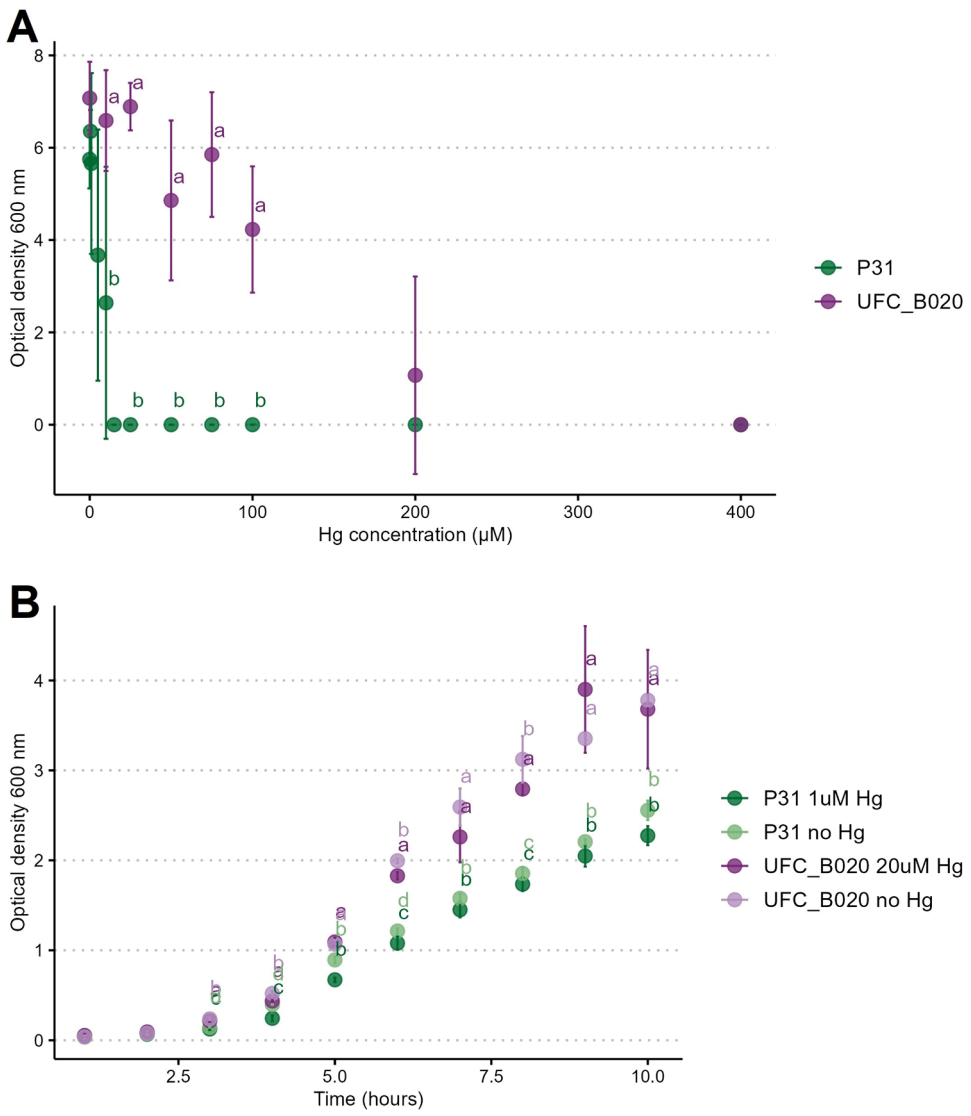

Fig. 1. **(A)** Bacterial growth of *UFC_B020* and *P31* at various Hg concentrations. OD_{600nm} of the culture medium was measured after 48 h of incubation at 30°C. **(B)** Growth curves of *UFC_B020* and *P31* in absence or presence of Hg. OD_{600nm} of the culture medium was measured over time of incubation at 30°C. Under Hg stress, concentrations correspond to the $MIC_{10\%}$ of each strain (20 µM for *UFC_020* and 1 µM for *P31* respectively). Error bars correspond to the standard deviation calculated from triplicates. Letters indicate significant differences between conditions according to Kruskal-Wallis test followed by Dunn analysis ($p < 0.05$).

Table 1
Growth kinetics parameters of *P31* and *UFC_B020* strains with or without Hg stress. For each parameter, the estimated value ± the standard error are provided. Quality metrics of the kinetic model are provided for each condition.

Condition	Growth rate (h^{-1})	Lag time (h)	Generation time (h)	R^2	Standard error of the fit	Residual variance
UFC_B020 0 µM Hg	1.59 ± 0.07	3.39 ± 0.13	0.44 ± 0.02	0.992	0.32	0.1022
UFC_B020 20 µM Hg	1.52 ± 0.13	3.50 ± 0.28	0.46 ± 0.04	0.959	0.717	0.5144
P31 0 µM Hg	0.82 ± 0.02	2.76 ± 0.09	0.84 ± 0.02	0.996	0.132	0.0175
P31 1 µM Hg	0.92 ± 0.04	3.46 ± 0.11	0.75 ± 0.03	0.994	0.152	0.023

The *UFC_B020* strain only appeared to respond significantly at a concentration of 100 µM Hg (Fig. 3**C**). At lower concentrations, there was no difference in intensity ratios compared to bacteria incubated with the ATC-Hg probe alone. This is consistent with the results described above, since *UFC_B020* seemed to have the ability to rapidly volatilise Hg in the medium at concentrations of 10 and 20 µM. At 100 µM, the amount of Hg present in the medium was greater and therefore the incubation time of 5 min may not be sufficient to volatilise Hg, resulting in a higher intensity ratio. Conversely, for strain *P31*, there was a clear increase in the fluorescence signal at all Hg concentrations tested. However, no dose-dependent relationship was observed between Hg concentration and fluorescence intensity ratio: this could be explained by the mechanisms of Hg assimilation that are fortuitous and therefore not proportional to the environmental Hg concentration.

Variations in the incubation conditions of bacteria with Hg and ATC-Hg showed that when *UFC_B020* was incubated for 30 min with 20 µM Hg, there was a significant decrease in the fluorescence signal, which was consistent with the Hg measurements in the medium, since Hg remaining part was less than 50% for this strain after 30 min of exposure (Fig. 3**D**). On the *P31* side, an increase in incubation time with Hg

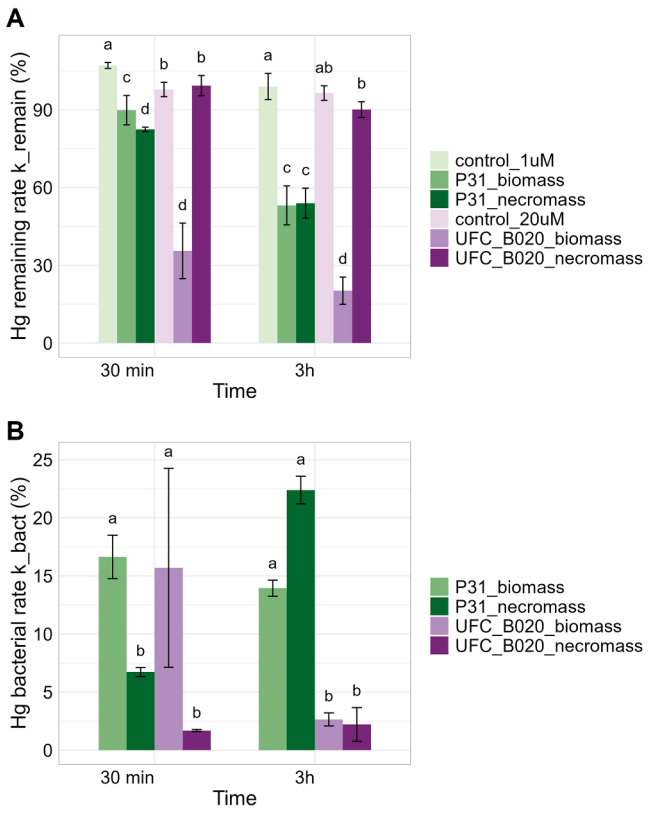

Fig. 2. Barplots representing **(A)** the Hg remaining rate k_{remain} and **(B)** the Hg bacterial rate k_{bact} after different conditions of incubation for 30 min or 3 h. Hg concentrations were set to the $MIC_{10\%}$ of each strain (20 μM for *UFC_B020* and 1 μM for *P31* respectively) and controls were incubated without bacterial material. Error bars correspond to the standard deviation calculated from triplicates. Letters indicate significant differences between conditions according to Kruskal-Wallis test followed by Dunn analysis ($p < 0.05$).

resulted in a significant increase in the intensity ratio.

3.4. Overview of RNA-Seq data and gene expression patterns

A summary of the sequencing statistics for RNA-Seq data is shown in **Table S1**. On average, 20.8 million clean reads were generated from each sample (20.8 ± 2.8 million reads, mean ± standard deviation, n = 24). Regarding *UFC_B020*, the total mapping rate and the unique mapping rate were 95.45% and 92.45% respectively. Regarding *P31*, the total mapping rate and the unique mapping rate were 99.08% and 98.10% respectively. In addition, GC content was constant across samples and the Q20 and Q30 were above 90% for all samples, which indicates that the sequencing data was of high quality and that there had been no contamination of the samples.

The gene expression patterns were investigated in the absence or presence of Hg, after two exposure periods for both *UFC_B020* and *P31* strains. A PCA was performed and explained 51.6% of the variability in the data (Fig. 4**A**). The first principal component (Dim1, 30.6%) mainly separated the exposure times (t1 = 30 min and t2 = 3 h), while the second principal component (Dim2, 21%) mainly separated the two strains studied. Incubation time predominantly affected the composition of expressed genes, as the samples were primarily grouped by exposure time. Within each time group, vertical separation was observed between strains, suggesting that genetic differences between strains were the second factor of variation, leading to distinct expression profiles between *P31* and *UFC_B020*. Time-dependent developmental or physiological changes appeared to be more significant than the response to Hg-induced stress; the latter may be more specific and targeted, affecting a smaller number of genes that do not dominate the overall variance.

K-means clustering was performed on the top 400 genes with the lowest standard deviation for their expression levels to group together genes with similar transcriptional signatures. Each cluster represented a functional "module" of potentially co-regulated genes (Fig. 4**B**). There were clear differences between the various conditions, and replicates within the same condition demonstrated homogeneity. Cluster 1 exhibited a highly specific expression signature to the *P31* strain exposed to Hg for 30 min, characterised by strong overexpression, which could represent a rapid response to Hg stress. The *UFC_B020* strain under the same conditions also showed overexpressed genes, albeit with less contrast. Moreover, cluster 3 comprised a small number of genes that were overexpressed in both strains in the presence of Hg, at both exposure times tested. Therefore, these genes must be directly involved in specific response mechanisms to cope with Hg stress. Cluster 2 showed a clear separation between the two strains: irrespective of Hg treatment and exposure time, gene overexpression was observed for strain *P31*. In a similar way to cluster 2, cluster 5 highlighted gene overexpression in *P31* and underexpression in *UFC_B020*, although at a lower intensity. In contrast to clusters 2 and 5, there was an overexpression of genes for strain *UFC_B020* in cluster 4, corresponding to a characteristic differential expression signature between the two strains. In cluster 6, gene expression showed an alternating pattern based mainly on exposure time (t1 *vs* t2). Therefore, there was a signature of genes regulated by exposure time more than by strain or Hg stress. The reverse expression pattern of cluster 7 indicated that temporal effects, independent of other experimental variables, influenced the regulation of gene expression.

Fig. 4**C** illustrates the main pathways associated with enriched BP subontologies as networks for different clusters. Cluster 1, which showed specific overexpression in *P31* and *UFC_B020* in the presence of Hg after 30 min Hg exposure, comprised genes mainly associated with nucleotide metabolism and protein repair. More specifically, the processes involved were the biosynthesis and metabolism of dTMP and dTTP, and the organisation and repair of protein complexes, redox processes and electron transport chains. All this suggests a response of DNA and protein protection to Hg-induced stress. Cluster 3 had a dense network of transport pathways for inorganic ions, cations, transition metals, and metal ions. The enrichment of ion transporters is consistent with a response to Hg stress, as indicated by the expression signature on the heatmap. These genes are likely to be involved in cellular detoxification and metal ion homeostasis. Energy metabolism and catabolism processes were enriched in cluster 6, which is consistent with an adaptive response to changes in energy processes over time, irrespective of the strain or the presence of Hg. Finally, cluster 7 appeared to be associated with phosphate homeostasis and protein quality control. This analysis of the main enriched BP pathways confirmed that the transcriptomic response observed was biologically coherent, with distinct functional clusters corresponding to different aspects of adaptation and response to Hg stress, with variations depending on the strain and exposure time.

3.5. Differentially expressed genes identification and gene functional enrichment analysis

DEGs were identified for each strain at each time step by comparing conditions with and without Hg exposure, with the following parameters: $|\log_2\text{FoldChange}| > 1.5$ and FDR < 0.05. For *UFC_B020*, there were 25 up-regulated and 3 down-regulated DEGs after 30 min Hg exposure (Fig. 5**A**), and 16 up-regulated and 5 down-regulated DEGs after 3 h (Fig. 5**B**). The number of DEGs decreased slightly after 3 h, but the $\log_2$FoldChange ($\log_2$ FC) remained similar. After 30 min Hg exposure, the most enriched GO term for BP was metal ion transport (GO:0030001). Regarding Molecular Function (MF) GO terms, transmembrane transporter activity (GO:0022857) and transporter activity (GO:0005215) were the two significantly enriched pathways (Fig. 6**A**).

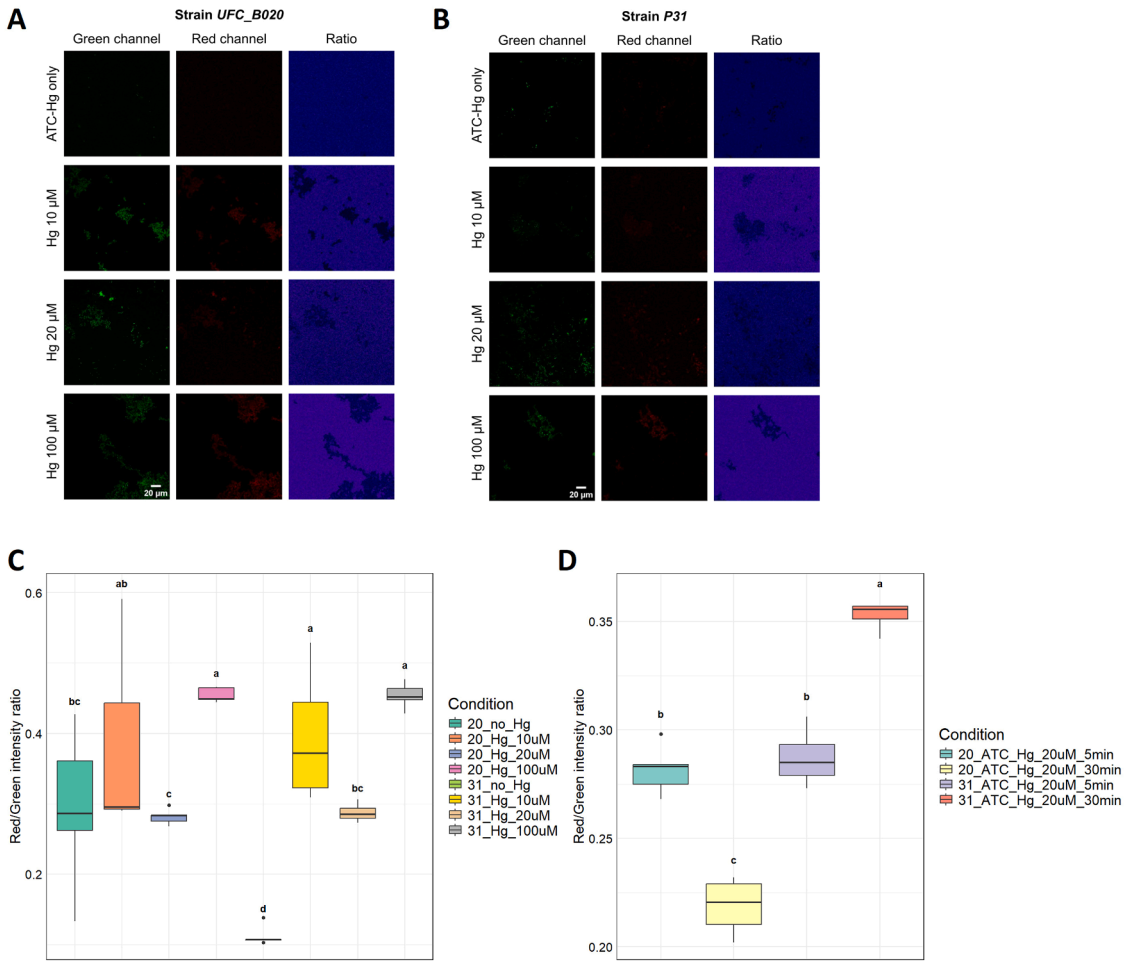

Fig. 3. Fluorescent two-photon microscopy images of **(A)** *UFC_B020* and **(B)** *P31* treated with 5 µM ATC-Hg for 5 min and various Hg concentrations (0, 10, 20 and 100 µM) for 5 min. Ratio images correspond to the image ratio of red/green channels. Image acquisition was performed with a Nikon A1-MP scanning microscope equipped with a Plan APO IR × 60 objective and the excitation wavelength of the laser was set to 810 nm. For each condition, the ATC-Hg concentration was 5 µM. The scale bar represents a length of 20 µm. **(C)** Average intensity ratios from ratio images of *UFC_B020* and *P31* at various Hg concentrations. **(D)** Average intensity ratios from ratio images of *UFC_B020* and *P31* incubated with ATC-Hg and Hg under various conditions. Each intensity ratio has been calculated from a minimum of 3 images. Letters indicate significant differences between conditions according to Kruskal-Wallis test followed by Dunn analysis ($p < 0.05$).

After 3 h Hg exposure, no GO terms were significantly enriched regardless of the subontology. This can be explained by the low number of DEGs, which were scattered across different GO categories. Whether after 30 min or 3 h of exposure to Hg, no KEGG pathways were enriched in *UFC_B020* compared to the control condition without Hg stress.

For *P31*, there were 60 up-regulated and 8 down-regulated DEGs after 30 min Hg exposure (Fig. 5**C**), and 49 up-regulated and 3 down-regulated DEGs after 3 h (Fig. 5**D**). In contrast to *UFC_B020*, there were more DEGs, and $\log_2$ FC values showed greater amplitude, especially for up-regulated genes. After 30 min, no GO terms were significantly enriched, suggesting that the response mechanisms to Hg stress in *P31* were diffuse. Regarding KEGG enrichment, after 30 min, the two-component system pathway (ppu02020) was enriched (Fig. 6**C**). After 3 h, the organonitrogen compound catabolic process (GO:1901565) was the only significantly enriched GO term and the related DEGs were mainly involved in cell wall catabolism and allantoin degradation for a potential source of nitrogen (Fig. 6**B**). Histidine metabolism (ppu00340) and bacterial chemotaxis (ppu02030) KEGG pathways were also enriched in *P31*.

3.6. Comparison of strain-specific molecular responses

A linear regression analysis of the DEGs between *UFC_B020* and *P31* under Hg stress yielded R^2 values of 0.139 and 0.098 after 30 min and 3 h of Hg exposure, respectively (Fig. 7). There were 12 common DEGs between *UFC_B020* and *P31* after 30 min, and 9 after 3 h. Nearly half of *UFC_B020* DEGs overlapped with *P31*, which nonetheless exhibited a broader transcriptional response. KEGG enrichment analysis comparing *UFC_B020* to *P31* under Hg stress highlighted that the sulphur metabolism pathway (ppu00920) was enriched after 30 min Hg exposure and the ABC transporters pathway (ppu02010) was enriched after 3 h, respectively.

4. Discussion

The genus *Pseudomonas* is ubiquitous, with numerous species demonstrating a remarkable ability to withstand environmental stresses (Silby et al., 2011). In this study, we compared Hg resistance levels between two *Pseudomonas canadensis* strains: *P31*, isolated from a salt marsh, and *UFC_B020*, isolated from Hg-contaminated soil.

4.1. Contrasting Hg resistance levels and detoxification strategies between UFC_B020 and P31

The two strains exhibited markedly different Hg resistance levels, with *UFC_B020* capable of growing at Hg concentrations up to 20-fold higher than *P31*. This finding suggests that environmental selection pressure from the Hg-contaminated habitat led to enhanced Hg

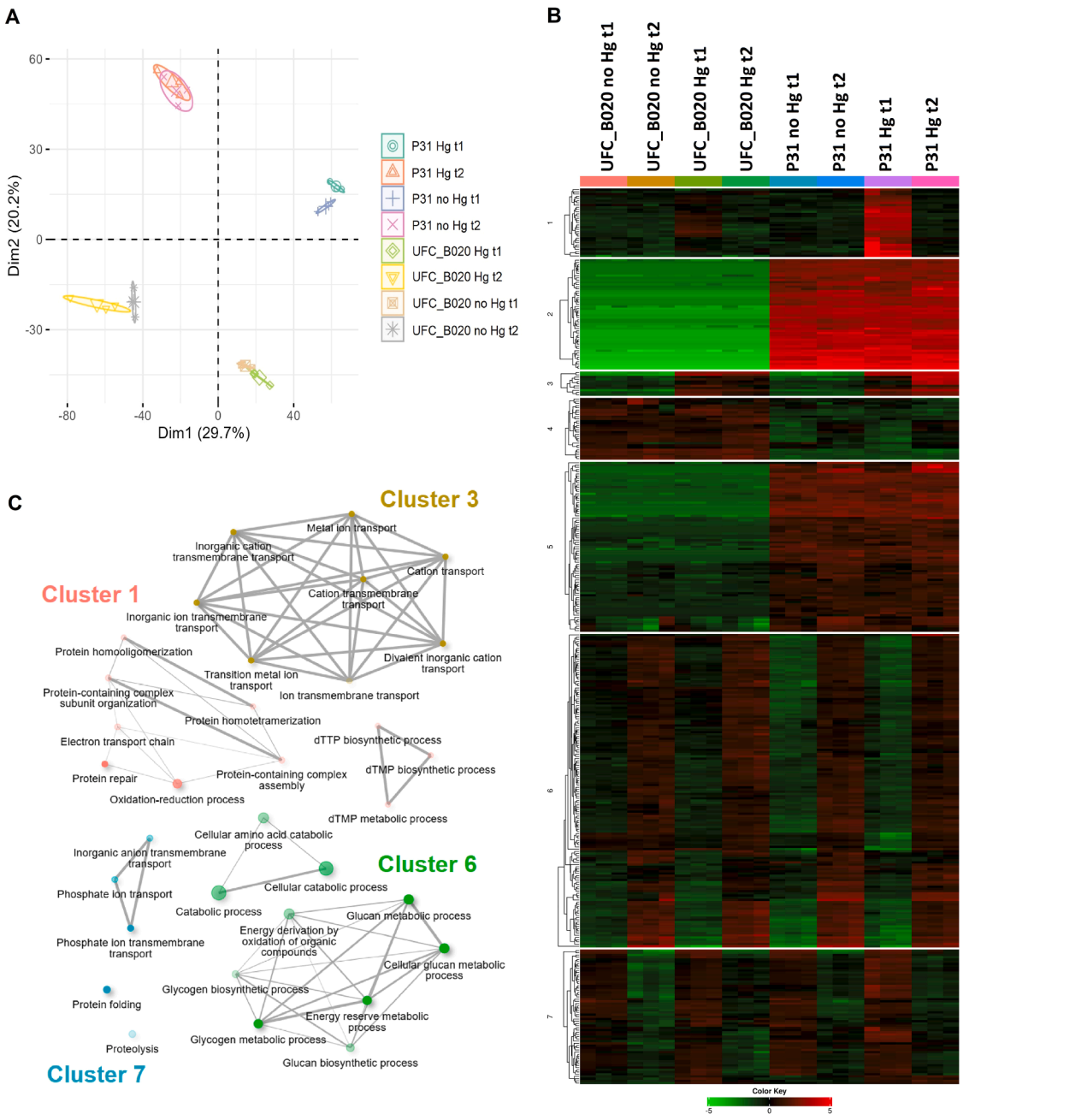

Fig. 4. Global expression pattern and GO enrichment in BP across gene clusters. **(A)** Principal component analysis plot of the estimated gene expression levels (based on counts of Fragments Per Kilobase of transcript sequence per Millions base pair-sequenced). Each point corresponds to a replicate, and replicates of the same condition are clustered by a coloured ellipse which delineate the 95% confidence intervals. **(B)** K-means clustering of the top 400 genes with the lowest standard deviation for their expression levels. Genes whose expressions were greater than the mean are coloured red while those below the mean are coloured green. Each column represents a specific condition (with 3 replicates per condition) and the dendrogram on the left shows the distance between genes. **(C)** Networks of main pathways associated with some clusters of genes, based on GO enrichment for BP subontology.

resistance mechanisms in *UFC_B020*. In contrast, strain *P31* comes from an uncontaminated environment, which may explain the lag time observed during bacterial growth, suggesting that Hg has deleterious effects on cell machinery. Deng and Wang (2012) observed similar patterns in the growth of *Pseudomonas* sp. S1 after exposure to MeHg. However, exposure to Hg did not affect the growth of *UFC_B020* at the lowest Hg concentrations, confirming its high level of resistance. Previous studies have documented the prevalence of *Pseudomonas* species in Hg-contaminated environments, and resistance to Hg has also been observed in the *Pseudomonas* genus at similar concentrations, highlighting its adaptive capacity under metal stress conditions (Chen et al., 2018b; Giovanella et al., 2015). For example, the *P. alkylphenolica* KL28 strain was able to withstand Hg concentrations of up to 100 μM by accumulating it within the cells (Shi et al., 2019). Furthermore, Hg reduction and volatilisation mechanisms have been identified in certain *Pseudomonas* strains, including *Pseudomonas* strain K-62 (Sone et al., 2013).

As there was no difference between Hg amounts in biomass and necromass for *P31*, Hg may have been passively taken up by bacterial cells or adsorbed onto bacterial cell walls. The passive uptake phenomenon via Hg biosorption was studied and characterised in the *Brevundimonas IITISM22* strain, which was found to have a high affinity for

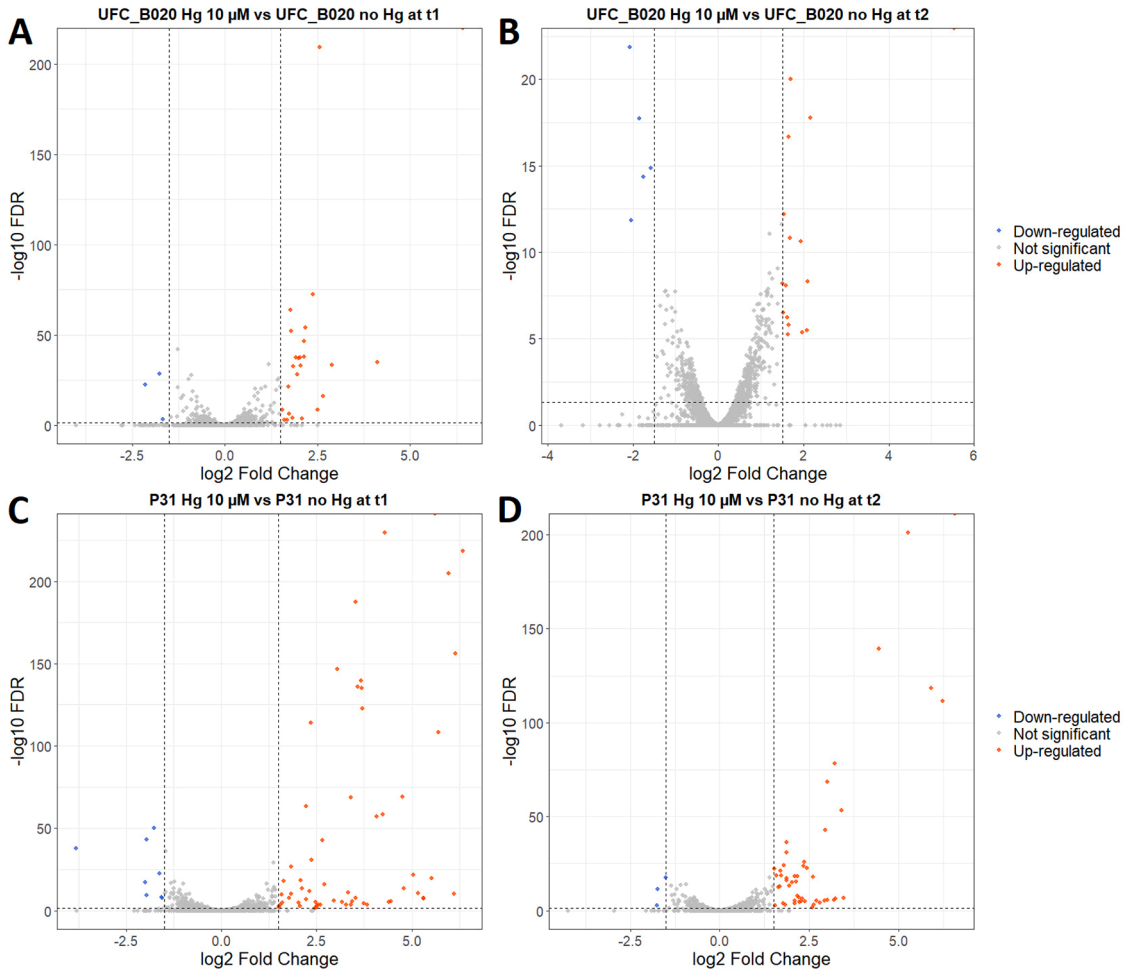

Fig. 5. Differential gene expression of *UFC_B020* and *P31* strains under Hg stress across exposition time. **(A)** Volcano plot showing DEGs in *UFC_B020* after 30 min (t1) of Hg exposition in comparison to the same conditions without Hg. **(B)** Volcano plot showing DEGs in *UFC_B020* after 3 h (t2) of Hg exposition in comparison to the same conditions without Hg. **(C)** Volcano plot showing DEGs in *P31* after 30 min (t1) of Hg exposition in comparison to same conditions without Hg. **(D)** Volcano plot showing DEGs in *P31* after 3 h (t2) of Hg exposition in comparison to the same conditions without Hg. Orange spots indicate significant up-regulated genes after Hg exposure; blue spots indicate significantly down-regulated genes. DEGs were screened with the following criteria: $|\log_2 \text{Foldchange}| > 1.5$ and FDR < 0.05.

Hg ions when used as an adsorbent for detoxification (Singh et al., 2021). Conversely, the proportion of Hg taken up by the *UFC_B020* biomass increased after 30 min of exposure and then decreased after 3 h. In the case of necromass, there was no Hg uptake, regardless of the duration of exposure, as Hg bacterial rate k_{bact} was practically zero. This suggests that biovolatilisation process occurred, with nearly 75% of the Hg present in the environment removed from the medium, as there did not appear to be any extracellular adsorption or intracellular accumulation. The *Pseudomonas* genus has previously been identified as being responsible for the biovolatilisation of Hg into its elemental form Hg^0, and *Pseudomonas* strains have therefore been considered a promising bioremediation tool on several case studies (Chang et al., 2021; Chen et al., 2018b). Here, characterisation of Hg resistance mechanisms through evaluation of Hg remaining rate k_{remain} and Hg bacterial rate k_{bact} following incubation with bacterial biomass or necromass revealed distinct detoxification strategies between the two strains. *UFC_B020* demonstrated active Hg removal, likely through biovolatilisation, whereas *P31* exhibited passive cellular mechanisms to cope with Hg toxicity. The latter strain showed evidence of Hg adsorption/accumulation, explaining the observed decrease in medium concentration, albeit significantly lower than that observed with *UFC_B020*.

The two-photon microscopy observations using the ATC-Hg fluorescent probe corroborated previous findings. Following 30 min of Hg exposure, *UFC_B020* showed decreased fluorescence intensity ratios, which is consistent with Hg volatilisation. Conversely, prolonged Hg incubation of *P31* resulted in increased fluorescence signals. Neither strain exhibited dose-dependent responses to increasing Hg concentrations, suggesting saturation or threshold effects rather than proportional responses. Strain *P31* demonstrated potential for binary Hg detection, showing significant fluorescence increases even at 10 µM Hg: its inability to volatilise Hg over time makes it a promising candidate for bacterial biosensor development.

Other studies have confirmed the role of environmental conditions in the rapid evolution and selection of genes involved in resistance to contaminants, particularly metals and antibiotics (Jia et al., 2022; Zhang et al., 2022). Studies have shown the implications of horizontal gene transfer in the acquisition of Hg resistance genes within microbial communities, and the structure of the latter may be significantly affected by Hg pollution (Hall et al., 2020). In our study, we focused on individual strains, but it would be relevant to study the interactions and exchanges that could occur between *P31* and *UFC_B020*. The genome of *P31* was publicly available on NCBI, while that of *UFC_B020* was sequenced in this study, confirming its taxonomic affiliation to *P. canadensis*. The genomic sequences of the two strains were then aligned and compared, revealing 93.32% sequence similarity. These data showed that although the two strains are genetically similar, they differ by more than 6% at the genomic level, which may reflect their respective adaptations to their environments, particularly to Hg stress in

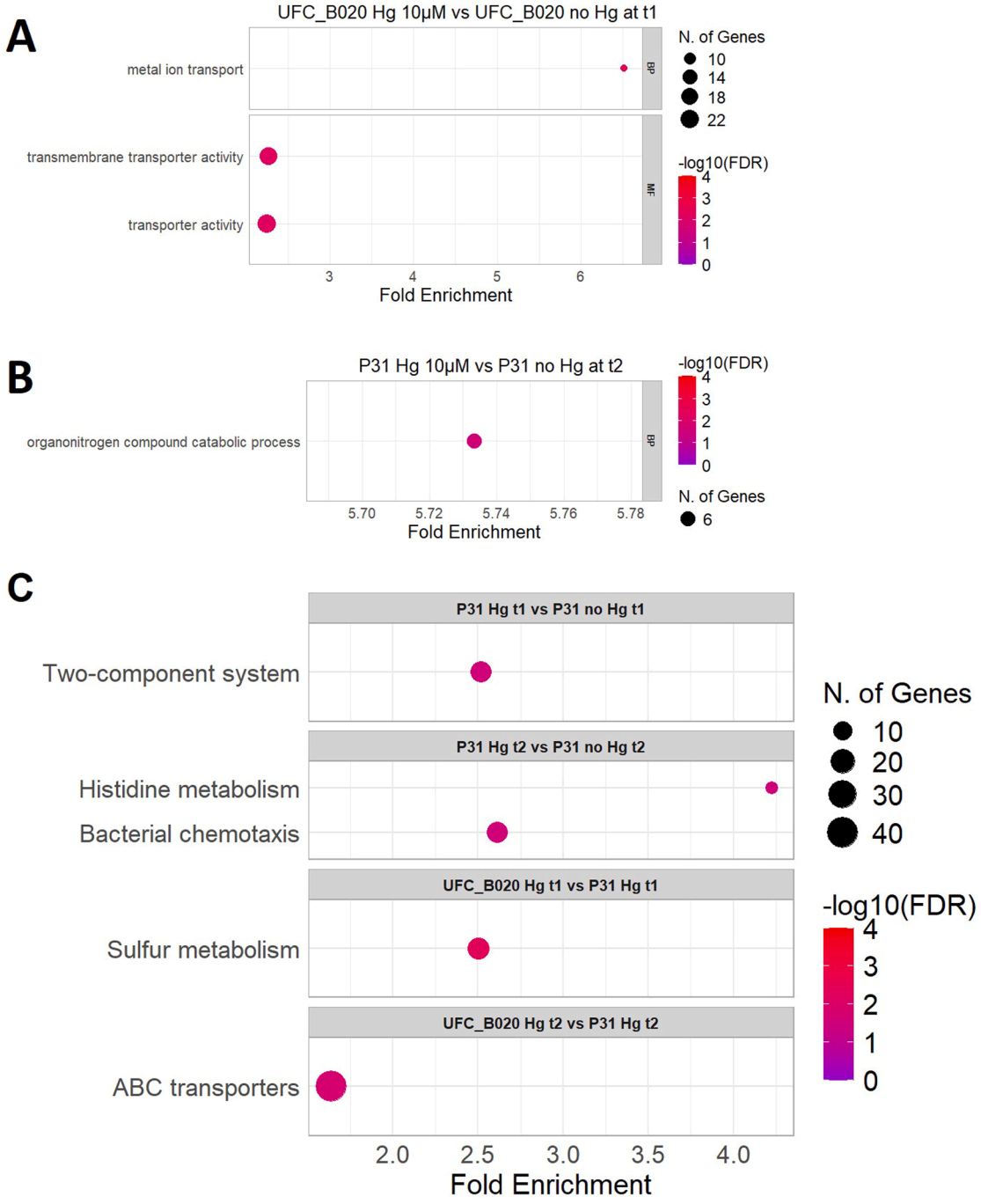

Fig. 6. (A) Dot plot showing the significantly enriched GO terms for *UFC_B020* under Hg stress vs no Hg stress after 30 min (t1). **(B)** Dot plot showing the significantly enriched GO term for *P31* under Hg stress vs no Hg stress after 3 h (t2). BP: biological process; MF: molecular function. **(C)** Dot plot showing the significantly enriched KEGG pathways for different comparisons. Each comparison is specified in the gray panel. DEGs for GO and KEGG enrichment were screened with the following criteria: $|\log_2 \text{Foldchange}| > 1.5$ and FDR < 0.05.

the case of *UFC_B020*.

4.2. Transcriptomic responses of P. canadensis strains following Hg exposure

The transcriptomic approach aimed to compare the response of *P31* and *UFC_B020* to Hg-induced stress, while considering their different levels of resistance. The concentrations selected for Hg exposure corresponded to 10% of the respective MIC of each strain, which avoided any growth impairment and ensured that both strains were exposed to a comparable level of stress in relation to their respective tolerances. RNA-Seq analysis revealed the molecular mechanisms underlying Hg resistance in both strains. This high-throughput sequencing technique has been previously applied to study metal-induced stress in *Pseudomonas*, including copper and zinc stress (Lei et al., 2020; Quintana et al., 2017) and bioremediation applications (Morales et al., 2021). To our knowledge, this work represents the first comparative transcriptomic study of Hg responses between *Pseudomonas* strains from two contrasting soils.

Gene clustering, DEGs analysis, GO and KEGG enrichment highlighted that there was an active Hg influx into cells for potential volatilisation by *UFC_B020* after short-term exposure, since the GO terms metal ion transport, transmembrane transporter activity and transporter

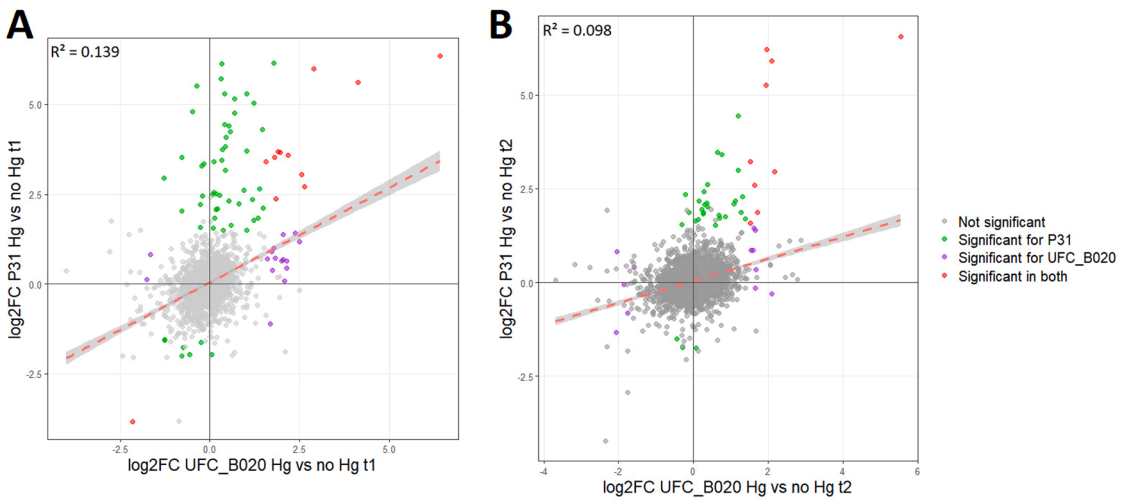

Fig. 7. Pairwise scatter plots of the $\log_2$ FC values of DEGs for *UFC_B020* and *P31* **(A)** after 30 min (t1) and **(B)** after 3 h (t2) following Hg exposure. DEGs were obtained by comparing gene expression levels of a given condition under Hg stress to the same condition without Hg exposure. Red spots indicate DEGs present in both strains; purple spots indicate DEGs present only in *UFC_B020*; green spots indicate DEGs present only in *P31*. DEGs were screened with the following criteria: $|\log_2\text{Foldchange}| > 1.5$ and FDR < 0.05. The plots were fitted with a linear regression, corresponding to the red dotted line, and R^2 values are shown on the respective graphs.

activity were significantly enriched. In the long term, the transcriptional response was more heterogeneous, but this may be explained by the fact that after 3 h of exposure, more than two-thirds of the Hg initially present in the medium was removed. There was therefore an effective and rapid detoxification of Hg by *UFC_B020*, which reduced cellular stress and perhaps the differential expression of certain molecular pathways. For *P31*, after 30 min of Hg exposure, the two-component system pathway was enriched: two-component systems are composed of a homodimeric sensor histidine kinase and a response regulator that can bind to DNA and regulate the expression of certain genes in response to environmental changes (Casino et al., 2010). The presence of Hg therefore appeared to induce a rapid signalling cascade in *P31*. In the long term, after 3 h of exposure to Hg, activation of cell division and inhibition of nitrogen molecules degradation were demonstrated (Uehara et al., 2008). Histidine metabolism and bacterial chemotaxis were also enriched pathways. Beyond its affinity for cysteines with thiol groups, it has been shown that Hg can also be chelated by imidazole groups of histidine residues (Stratton et al., 2016): thus, the complexes formed between Hg and histidines could disrupt the structure of certain proteins. In addition, the two-component systems that were enriched after 30 min exposure rely on histidine phosphorylation for signal transduction. It can therefore be assumed that in the longer term, the increased mobilisation of the two-component systems has led to an increase in histidine metabolism (Papon & Stock, 2019). Bacterial chemotaxis allows the detection of chemical gradients in the environment and can modify the motility of bacteria accordingly to optimise their position (Barrionuevo & Vullo, 2012). In the case of Hg-induced stress, this pathway can allow bacteria to migrate to a less contaminated area, with an avoidance strategy. Other studies have already observed that bacterial chemotaxis as well as the two-component systems were affected following Hg exposure in *P. stutzeri* (Zheng et al., 2018).

Overall, the transcriptomic response was more pronounced in *P31*, with greater numbers of DEGs and higher $\log_2$ FC for genes that were common to both strains (Table 2). Nevertheless, the experimental conditions differed between the 2 strains: *UFC_B020* was exposed to 20 μM Hg while *P31* was exposed to only 1 μM Hg, reflecting their respective resistance levels. Despite 20-fold lower Hg concentration, *P31* showed stronger transcriptional changes, consistent with its limited detoxification capacity. Both strains exhibited perturbations in sulphur metabolism and oxidative stress responses that are well-documented effects of Hg exposure (Rice et al., 2014). Again, these responses were more pronounced in *P31*. Numerous DEGs in both strains related to membrane transport and efflux systems for metal ions and diverse molecules, suggesting that extracellular metal export represents a potential Hg resistance mechanism. However, *UFC_B020* showed fewer transport-related

Table 2
Annotated differentially expressed genes (DEGs) common to *UFC_B020* and *P31* after 30 min (t1) and 3 h (t2) under Hg stress.

Gene name	Gene product description	$\log_2$ FC *UFC_B020*	FDR *UFC_B020*	$\log_2$ FC *P31*	FDR *P31*
Common DEGs at t1 (after 30 min Hg exposure)					
cadA	Cadmium, zinc and cobalt-transporting ATPase	6.42	0.00E+00	6.35	5.76E-219
qseC	Sensor protein	1.79	9.52E-53	3.53	3.06E-188
dsbG	Thiol:disulfide interchange protein	2.18	1.41E-54	3.59	1.26E-136
yneN	Thioredoxin-like protein	1.91	4.77E-38	3.69	8.23E-136
ceeh-1	Epoxyde hydrolase 1	1.95	8.32E-29	3.66	1.98E-140
thrS	Threonine–tRNA ligase	1.56	4.84E-09	3.41	3.36E-69
czcB	Cobalt-zinc-cadmium resistance protein	2.64	1.05E-16	2.71	1.07E-16
Common DEGs at t2 (after 3 h Hg exposure)					
cadA	Cadmium, zinc and cobalt-transporting ATPase	5.54	0.00E+00	6.56	0.00E+00
czcA	Cobalt-zinc-cadmium resistance protein	1.52	3.29E-07	3.22	4.12E-79
czcC	Cobalt-zinc-cadmium resistance protein	1.94	2.29E-11	5.27	9.57E-202
lolD	Lipoprotein-releasing system ATP-binding protein	1.51	6.73E-09	1.58	2.08E-19
czcB	Cobalt-zinc-cadmium resistance protein	1.96	4.16E-06	6.22	2.76E-112
folE2	GTP cyclohydrolase	1.64	5.47E-06	2.60	9.47E-19

DEGs, consistent with intracellular Hg biovolatilisation reducing the need for extensive efflux systems, as bacterial membranes are permeable to volatile Hg forms (Faucheur et al., 2013).

4.3. Strain-specific gene expression patterns

Gene expression profiles under Hg exposure showed poor correlation between the two strains, irrespective of exposure duration. Consequently, the number of DEGs following Hg stress varied considerably between strains, and even when DEGs were shared, their expression patterns remained strain-specific. Although both strains demonstrated overlapping Hg response mechanisms, they diverged markedly in response magnitude and employed distinct adaptive strategies. This distinction is crucial given that *P31* exhibited greater fold-changes in response to 1 μM Hg than *UFC_B020* displayed under 20 μM exposure, indicating differential Hg sensitivity and suggesting that *P31* experiences more pronounced transcriptional stress per unit of Hg concentration.

KEGG enrichment analysis comparing *UFC_B020* to *P31* under Hg stress highlighted sulphur metabolism pathway enrichment after 30 min Hg exposure and ABC transporters pathway enrichment after 3 h, respectively. Indeed, Hg has a strong affinity for thiol groups, which is partly responsible for its toxicity (Norambuena et al., 2017), and this could explain the increase in sulphur metabolism. Regarding ABC transporters, these are a family of membrane proteins that use ATP to transport various molecules, several of which have been identified as involved in metal transfer (Theodoulou & Kerr, 2015). Under Hg stress, the enrichment of sulphur metabolism and ABC transporter pathways suggests an integrated response to oxidative stress. Sulphur metabolism contributes to the biosynthesis of thiol-based antioxidants such as glutathione, which is essential for maintaining cellular redox homeostasis. Concurrently, ABC transporters may facilitate the export of Hg–thiol conjugates and other oxidized metabolites, thereby supporting detoxification and redox balance. Together, these pathways likely represent a coordinated metabolic adaptation to mitigate Hg-induced oxidative damage. *UFC_B020* therefore presents a potential capacity for Hg efflux and/or influx greater than P31, perhaps because it has more suitable resistance mechanisms. Furthermore, this active transport pathway favoured in *UFC_B020* is consistent with the results for k_{remain} and k_{bact} as well as microscopic observations.

At the gene level, *cadA* had the highest $\log_2$ FC for both strains (Table 2). This gene is involved in the active transport of metal ions (Co^{2+}, Zn^{2+}, Cd^{2+}) coupled with ATP hydrolysis. The *czcCBA* efflux system genes were also overexpressed in both strains, consistent with their interdependent expression with *cadA* as shown by Ducret et al. (2020) in *Pseudomonas aeruginosa*. All metal-related genes were up-regulated, whether for efflux, regulation of resistance mechanisms at the transcriptional level, or for magnesium and iron homeostasis which is consistent with the GO enrichment results for *UFC_B020*. However, the $\log_2$ FC of these metal ion-related genes was higher for *P31*, which contained arsenic resistance genes such as *arsB* and *arsC* (Fernández et al., 2014). The *P31* strain therefore appeared to possess the *ars* operon, in contrast to *UFC_B020* (**Tables S2** and **S3**). Furthermore, the *zntR* and *cueR* genes, which correspond to transcriptional regulators of genes involved in zinc and copper stress response mechanisms, respectively, were overexpressed in *UFC_B020*. These two genes are homologues of the MerR family, which is associated with the uptake and detoxification of metal ions (Fang & Zhang, 2021). In addition, several genes encoding transporters were overexpressed, particularly after 30 min Hg exposure and in greater numbers in *P31*. This may indicate the establishment of resistance mechanisms based on Hg efflux. The gene encoding the lipoprotein translocase LolD to the outer membrane was overexpressed in both *UFC_B020* and *P31* in the presence of Hg (Bei et al., 2022). In *P31*, efflux genes linked to antibiotic resistance, such as *acrE* and *opdE*, were differentially expressed. Co-selection of heavy metal and antibiotic resistance genes has been demonstrated, and their coexistence within a bacterial strain's genome can affect its resistance (Vats et al., 2022).

Some DEGs were also involved in processes regulating gene expression and genetic material repair. However, a much larger number of genes in this category were differentially expressed in *P31*, suggesting that Hg-induced stress was greater in this strain, which is consistent with the KEGG enrichment results. Furthermore, *msrPQ* genes were strongly up-regulated in *P31* in the presence of Hg after 30 min Hg exposure; these genes protect proteins from oxidative stress (Vergnes et al., 2022). Indeed, one of the harmful effects of Hg on cells is an increase in ROS production, which causes oxidative damage (Rice et al., 2014). The metabolism of sulphur molecules was also affected by the presence of Hg as shown by KEGG enrichment analysis. The *yneN* and *dsbG* genes, which exhibit antioxidant activity, were differentially expressed in both *P31* and *UFC_B020*. Only *P31* contained additional genes associated with thiol-containing molecules. These were highly overexpressed only after 30 min, indicating that the presence of Hg in the environment rapidly affects sulphur metabolism. Finally, the *qseC* gene, which is involved in quorum sensing and the regulation of flagella assembly, was found to be upregulated after a 30 min exposure in both strains (Sperandio et al., 2002). In the longer term, the *bdlA* gene, which encodes a biofilm dispersion protein in *P31*, was also overexpressed. Hg was therefore found to affect cell motility and quorum sensing, which is consistent with another study by Zheng et al. (2018), which showed that Hg resistance genes are involved in inhibiting biofilm formation and flagellum development.

4.4. Demonstration of mer-independent detoxification mechanisms

Both strains exhibited substantial transcriptomic responses to Hg exposure, but with distinct expression patterns confirming strain-specific resistance strategies (Fig. 4). Notably, no *mer* operon genes were identified among DEGs, suggesting that resistance mechanisms operate independently of this classical detoxification system in both strains. Bacterial Hg biovolatilisation has been documented across several genera (Agarwal et al., 2019; Chang et al., 2019; Lefebvre et al., 2006) and was typically associated with the *merA* gene encoding mercuric reductase, which converts Hg^{2+} to volatile Hg^0 (Dash et al., 2017). However, Hg volatilisation has also been demonstrated in microorganisms lacking the *mer* operon (Lavoie & Poulain, 2025; Wiatrowski et al., 2006), which appeared to be the case for *UFC_B020*. Indeed, genes identified as corresponding to *merA* were found in the genomic data of *UFC_B020*, but were not differentially expressed under Hg stress (**Table S4**), and no other genes from the *mer* operon could be identified, confirming that the mechanisms of Hg resistance in *UFC_B020* are *mer*-independent, which is the first time this has been observed within the genus *Pseudomonas*. Generating mutants and conducting a more detailed study of the DEGs in *UFC_B020* in the presence of Hg would enable the identification of potential candidates involved in Hg biovolatilisation pathways. Recently, Lavoie and Poulain (2025) hypothesized that cellular thiols are key interaction sites mediating Hg reduction: although the exact cellular components remain unidentified, these are relevant avenues for elucidating Hg biovolatilisation independent of the *mer* operon, given the KEGG pathways and enriched GO terms highlighted in this study. Given the atmospheric persistence of Hg, biovolatilisation processes would enhance its environmental mobility, thereby extending contamination in uncontaminated ecosystems which is not intended for bioremediation purposes.

4.5. Limitations and future perspectives

The relatively modest number of DEGs under our experimental conditions, combined with limited gene annotations, resulted in few significantly enriched GO terms and KEGG pathways. While GO and KEGG enrichment analysis provides broad overviews of affected biological processes, individual DEG analysis enables more precise

understanding of specific molecular mechanisms. However, differential expression of individual genes does not necessarily indicate pathway-level perturbations, and DEG interpretation requires careful consideration of broader regulatory networks.

Fig. 8 proposes a model of response to Hg-induced stress that is specific to each of the two *P. canadensis* strains. This model highlights the contrasting cellular-level effects of Hg depending on the level of resistance. Further refinement of this model at the molecular level could elucidate the biovolatilisation mechanisms in *UFC_B020*, which do not rely on the *mer* operon unlike what is often the case in bacteria. Additionally, validation of transcriptomic findings through proteomics and metabolomics approaches would provide a more comprehensive understanding of strain-specific Hg resistance mechanisms: this would provide new insights into the role of microorganisms, particularly the *Pseudomonas* genus, in the biogeochemical cycle of Hg. For bioremediation purposes, it would be relevant to enhance the tolerance of strains of interest by gradually increasing the Hg stress concentration: these acclimatisation phases would thus optimise the decontamination processes. Overall, this work confirmed that the search for endogenous microbial candidates may be promising, since the selection pressure exerted by contaminants in contaminated soils allows for genetic adaptation as well as for acquisition of resistance and detoxification mechanisms that can be used in a tailored manner.

5. Conclusions

This study compared the response to Hg stress in two strains of *Pseudomonas canadensis: UFC_B020*, which was isolated from a Hg-contaminated medium, and *P31*, which was isolated from an unpolluted matrix. Using multiple experimental approaches, including monitoring Hg transfer processes in the presence of biomass and bacterial necromass, as well as through microscopic observations and RNA-Seq, we were able to characterise the processes involved in Hg detoxification at the cellular and molecular levels, and assess their effectiveness. The *UFC_B020* strain exhibited a significantly greater ability to withstand Hg stress than *P31*; the former displayed active resistance mechanisms, such as biovolatilisation, whereas the latter exhibited passive and compensatory mechanisms in response to Hg toxicity. In particular, almost no genes belonging to the *mer* operon were identified in *UFC_B020*, and none of them were differentially expressed, suggesting that the detoxification pathways in this strain rely on *mer*-independent mechanisms, which, to date, had not been demonstrated in a *Pseudomonas* species. Despite their high genomic similarity, these results demonstrated how environmental conditions can impact the selection of Hg resistance genes and provided insights into the responses to Hg stress in the *Pseudomonas* genus.

Funding sources

The project BIOSYSMO has received funding from the European Union's Horizon Europe research and innovation program under grant agreement n°101060211. This work has been supported by TRANSBIO Graduate School (contract ANR-15-IDEX-0003) and the Region Bourgogne-Franche-Comte.

Data availability

The data presented in this study are available within the article and supplementary materials. The genome data of *UFC_B020* have been deposited at NCBI under BioProject accession number PRJNA1308019 and the BioSample accession number is SAMN50679194. The Illumina sequencing reads are available in the NCBI Sequence Read Archive under accession SRR35033844. The genome data of *P31* are available in the NCBI public repository, with the accession number GCA_963970765.1. *Pseudomonas canadensis* RNA sequence reads data are available in the NCBI public repository, with the accession number PRJNA1277159.

CRediT authorship contribution statement

Lorraine Meyer: Writing – review & editing, Writing – original draft, Methodology, Formal analysis, Data curation, Conceptualization. **Jun Zhou:** Writing – review & editing, Resources, Project administration, Methodology. **Stéphane Pfendler:** Writing – review & editing, Supervision, Resources, Methodology. **Siyu Mei:** Writing – review & editing, Resources. **Miao Wang:** Writing – review & editing, Resources. **Nicolas Capelli:** Writing – review & editing, Supervision, Resources, Project administration, Funding acquisition. **Stéphane Guyot:** Writing – review & editing, Supervision, Resources, Project administration. **Michel Chalot:** Writing – review & editing, Supervision, Resources, Project administration, Funding acquisition.

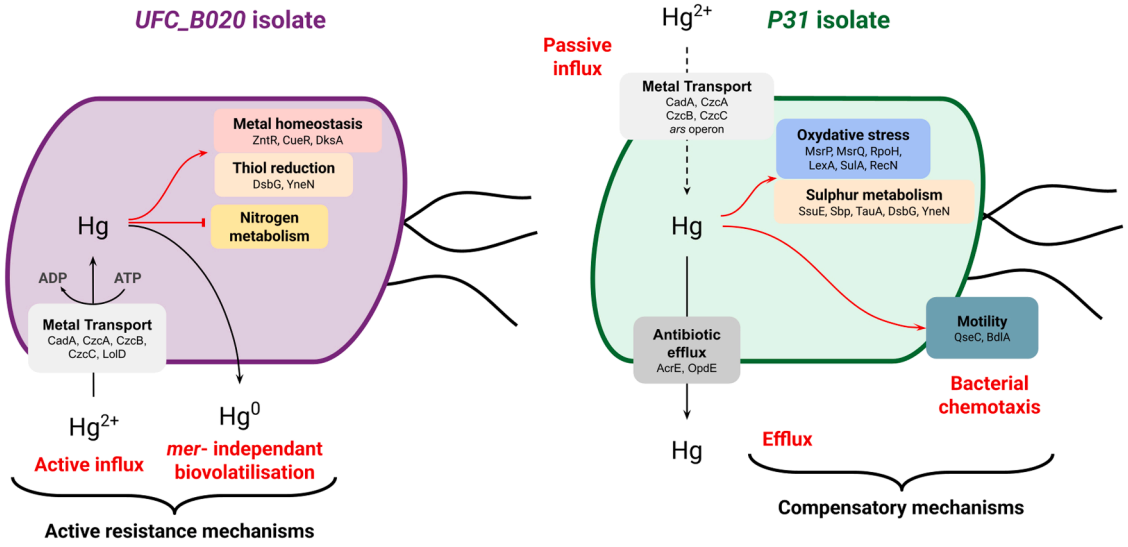

Fig. 8. Proposed model depicting the main pathways of responses to Hg stress in *UFC_B020* (left) and *P31* (right). Red arrows denote the effects of Hg on metabolic pathways while black arrows represent Hg transfers. The proteins and genes involved in a given cellular pathway are indicated in the associated coloured box. ATP: Adenosine triphosphate.

Declaration of competing interest

The authors declare that they have no known competing financial interests or personal relationships that could have appeared to influence the work reported in this paper.

Acknowledgments

We would like to express our sincere thanks to Jolanda Brons of the University of Groningen for providing us with the *Pseudomonas canadensis P31* strain. We also thank the DImaCell imaging facility (Institut Agro Dijon, INRAE, Université Bourgogne Europe, Université Marie et Louis Pasteur, F-21000 Dijon, France) and the PEA²t platform (Université Marie et Louis Pasteur, Chrono-environnement, F-25000 Besançon, France) for technical support.

Supplementary materials

Supplementary material associated with this article can be found, in the online version, at doi:10.1016/j.hazadv.2026.101069.

References

Agarwal, M., Rathore, R.S., Jagoe, C., Chauhan, A., 2019. Multiple lines of evidences reveal mechanisms underpinning mercury resistance and volatilization by *Stenotrophomonas* sp. MA5 isolated from the Savannah river site (SRS), USA. Cells 8 (4), 309. https://doi.org/10.3390/cells8040309.

Al-Ansari, M.M., Benabdelkamel, H., AlMalki, R.H., Rahman, A.M.A., Alnahmi, E., Masood, A., Ilavenil, S., Choi, K.C., 2021. Effective removal of heavy metals from industrial effluent wastewater by a multi metal and drug resistant *Pseudomonas aeruginosa* strain RA-14 using integrated sequencing batch reactor. Environ. Res. 199, 111240. https://doi.org/10.1016/j.envres.2021.111240.

Alfarras, A.F., Al-Fahdawi, M.H., Albayaty, M.K., 2022. Heavy metal resistance ability of *Pseudomonas* species isolated from sludge and sewage in Iraq. DOAJ (DOAJ: Directory Open Access J.) 77 (3), 1041–1047. https://doi.org/10.22092/ari.2022.357399.2036.

Anders, S., Pyl, P.T., Huber, W., 2014. HTSeq—a Python framework to work with high-throughput sequencing data. Bioinformatics 31 (2), 166–169. https://doi.org/10.1093/bioinformatics/btu638.

Aschner, M., Syversen, T., Souza, D.O., Rocha, J.B., 2006. Metallothioneins: mercury species-specific induction and their potential role in attenuating neurotoxicity. Exp. Biol. Med. 231 (9), 1468–1473. https://doi.org/10.1177/153537020623100904.

ATSDR, 2017. Substance priority list agency for toxic substances and disease registry.

Bateman, A., Martin, M., Orchard, S., Magrane, M., Ahmad, S., Alpi, E., Bowler-Barnett, E.H., Britto, R., Bye-A-Jee, H., Cukura, A., Denny, P., Dogan, T., Ebenezer, T., Fan, J., Garmiri, P., Da Costa Gonzales, L.J., Hatton-Ellis, E., Hussein, A., Ignatchenko, A., et al., 2022. UniProt: the universal protein knowledgebase in 2023. Nucleic Acids Res. 51 (D1), D523–D531. https://doi.org/10.1093/nar/gkac1052.

Barrionuevo, M.R., Vullo, D.L., 2012. Bacterial swimming, swarming and chemotactic response to heavy metal presence: which could be the influence on wastewater biotreatment efficiency? World J. Microbiol. Biotechnol. 28 (9), 2813–2825. https://doi.org/10.1007/s11274-012-1091-5.

Bei, W., Luo, Q., Shi, H., Zhou, H., Zhou, M., Zhang, X., Huang, Y., 2022. Cryo-EM structures of LolCDE reveal the molecular mechanism of bacterial lipoprotein sorting in *Escherichia coli*. PLoS Biol. 20 (10), e3001823. https://doi.org/10.1371/journal.pbio.3001823.

Bourdineaud, J., Durn, G., Režun, B., Manceau, A., Hrenović, J., 2020. The chemical species of mercury accumulated by *Pseudomonas idrijaensis*, a bacterium from a rock of the Idrija mercury mine, Slovenia. Chemosphere 248, 126002. https://doi.org/10.1016/j.chemosphere.2020.126002.

Casino, P., Rubio, V., Marina, A., 2010. The mechanism of signal transduction by two-component systems. Curr. Opin. Struct. Biol. 20 (6), 763–771. https://doi.org/10.1016/j.sbi.2010.09.010.

Chang, J., Yang, Q., Dong, J., Ji, B., Si, G., He, F., Li, B., Chen, J., 2019. Reduction in Hg phytoavailability in soil using Hg-volatilizing bacteria and biochar and the response of the native bacterial community. Microb. Biotechnol. 12 (5), 1014–1023. https://doi.org/10.1111/1751-7915.13457.

Chang, J., Yan, Z., Dong, J., Wu, X., Meng, Z., Shi, Y., Chen, J., 2021. Mechanisms controlling the transformation of and resistance to mercury(II) for a plant-associated *Pseudomonas* sp. strain, AN-B15. J. Hazard. Mater. 425, 127948. https://doi.org/10.1016/j.jhazmat.2021.127948.

Chen, S., Zhou, Y., Chen, Y., Gu, J., 2018a. fastp: an ultra-fast all-in-one FASTQ preprocessor. Bioinformatics 34 (17), i884–i890. https://doi.org/10.1093/bioinformatics/bty560.

Chen, J., Dong, J., Chang, J., Guo, T., Yang, Q., Jia, W., Shen, S., 2018b. Characterization of an Hg(II)-volatilizing *Pseudomonas* sp. strain, DC-B1, and its potential for soil remediation when combined with biochar amendment. Ecotoxicol. Environ. Saf. 163, 172–179. https://doi.org/10.1016/j.ecoenv.2018.07.071.

Chen, S., 2023. Ultrafast one-pass FASTQ data preprocessing, quality control, and deduplication using fastp. iMeta 2 (2). https://doi.org/10.1002/imt2.107.

Dash, H.R., Sahu, M., Mallick, B., Das, S., 2017. Functional efficiency of MerA protein among diverse mercury resistant bacteria for efficient use in bioremediation of inorganic mercury. Biochimie 142, 207–215. https://doi.org/10.1016/j.biochi.2017.09.016.

Deng, X., Wang, P., 2012. Isolation of marine bacteria highly resistant to mercury and their bioaccumulation process. Bioresour. Technol. 121, 342–347. https://doi.org/10.1016/j.biortech.2012.07.017.

Ducret, V., Gonzalez, M.R., Leoni, S., Valentini, M., Perron, K., 2020. The CzcCBA efflux system requires the CadA P-Type ATPase for timely expression upon zinc excess in *Pseudomonas aeruginosa*. Front. Microbiol. 11. https://doi.org/10.3389/fmicb.2020.00911.

Durand, M.J., Hua, A., Jouanneau, S., Cregut, M., Thouand, G., 2015. Detection of metal and organometallic compounds with bioluminescent bacterial bioassays. Adv. Biochem. Eng. Biotechnol. 77–99. https://doi.org/10.1007/10_2015_332.

Durand, A., Maillard, F., Foulon, J., Gweon, H.S., Valot, B., Chalot, M., 2017. Environmental metabarcoding reveals contrasting belowground and aboveground fungal communities from poplar at a Hg phytomanagement site. Microb. Ecol. 74 (4), 795–809. https://doi.org/10.1007/s00248-017-0984-0.

Fang, C., Zhang, Y., 2021. Bacterial MerR family transcription regulators: activation by distortion. Acta Biochem. Biophys. Sin. 54 (1), 25. https://doi.org/10.3724/abbs.2021003 (Shangai)36.

Faucheur, S.L., Campbell, P.G., Fortin, C., Slaveykova, V.I., 2013. Interactions between mercury and phytoplankton: speciation, bioavailability, and internal handling. Environ. Toxicol. Chem. 33 (6), 1211–1224. https://doi.org/10.1002/etc.2424.

Fernández, M., Udaondo, Z., Niqui, J., Duque, E., Ramos, J., 2014. Synergic role of the two ars operons in arsenic tolerance in *Pseudomonas putida* KT2440. Environ. Microbiol. Rep. 6 (5), 483–489. https://doi.org/10.1111/1758-2229.12167.

Ge, S.X., Son, E.W., Yao, R., 2018. iDEP: an integrated web application for differential expression and pathway analysis of RNA-Seq data. BMC Bioinform. 19 (1). https://doi.org/10.1186/s12859-018-2486-6.

Ghasemi, S., Harighi, B., Ashengroph, M., 2023. Biosynthesis of silver nanoparticles using *Pseudomonas canadensis*, and its antivirulence effects against *Pseudomonas tolaasii*, mushroom brown blotch agent. Sci. Rep. 13 (1). https://doi.org/10.1038/s41598-023-30863-x.

Giovanella, P., Cabral, L., Bento, F.M., Gianello, C., Camargo, F.A.O., 2015. Mercury (II) removal by resistant bacterial isolates and mercuric (II) reductase activity in a new strain of *Pseudomonas* sp. B50A. New Biotechnol. 33 (1), 216–223. https://doi.org/10.1016/j.nbt.2015.05.006.

Gworek, B., Dmuchowski, W., Baczewska-Dąbrowska, A.H., 2020. Mercury in the terrestrial environment: a review. Environ. Sci. Eur. 32 (1). https://doi.org/10.1186/s12302-020-00401-x.

Hall, J.P.J., Harrison, E., Pärnänen, K., Virta, M., Brockhurst, M.A., 2020. The impact of mercury selection and conjugative genetic elements on community structure and resistance gene transfer. Front. Microbiol. 11. https://doi.org/10.3389/fmicb.2020.01846.

Jia, J., Zhu, Z., Xue, X., Li, X., Wang, Z., 2022. Selective pressure governs the composition, antibiotic, and heavy metal resistance profiles of *Aeromonas* spp. isolated from Ba river in Northwest China. Environ. Sci. Pollut. Res. 29 (50), 75841–75850. https://doi.org/10.1007/s11356-022-20678-0.

Kanehisa, M., 2000. KEGG: Kyoto encyclopedia of genes and genomes. Nucleic Acids Res. 28 (1), 27–30. https://doi.org/10.1093/nar/28.1.27.

Kundlacz, C., Aldeia, C., Eddoubaji, Y., Campos-Madueno, E.I., Endimiani, A., 2024. Complete genome sequence of *Pseudomonas canadensis* strain Pcan-CK-23 isolated from *Zophobas morio* larvae. Microbiol. Resour. Announc. 13 (6). https://doi.org/10.1128/mra.00023-24.

Langmead, B., Salzberg, S.L., 2012. Fast gapped-read alignment with Bowtie 2. Nat. Methods 9 (4), 357–359. https://doi.org/10.1038/nmeth.1923.

LaVoie, S.P., Summers, A.O., 2018. Transcriptional responses of *Escherichia coli* during recovery from inorganic or organic mercury exposure. BMC Genomics 19 (1). https://doi.org/10.1186/s12864-017-4413-z.

Lavoie, N., Poulain, A., 2025. Anaerobic HgII reduction is driven by cellular HgII-thiol interactions. Access Microbiol. 7 (1). https://doi.org/10.1099/acmi.0.000932.v3.

Lefebvre, D.D., Kelly, D., Budd, K., 2006. Biotransformation of Hg(II) by cyanobacteria. Appl. Environ. Microbiol. 73 (1), 243–249. https://doi.org/10.1128/aem.01794-06.

Lei, L., Chen, J., Liao, W., Liu, P., 2020. Determining the different mechanisms used by *Pseudomonas* species to cope with minimal inhibitory concentrations of zinc via comparative transcriptomic analyses. Front. Microbiol. 11. https://doi.org/10.3389/fmicb.2020.573857.

Le Marc, Y., Coroller, L., 2025. Simulating bacterial growth and thermal inactivation with the Sym'Previus tool. In: Pérez-Rodríguez, F., Valero, A., Bolivar, A. (Eds.), Basic Protocols in Predictive Microbiology Softwares. Methods and Protocols in Food Science, Humana, New York, NY, pp. 107–121. https://doi.org/10.1007/978-1-0716-4112-5_5.

Li, H., Durbin, R., 2009. Fast and accurate short read alignment with Burrows–Wheeler transform. Bioinformatics 25 (14), 1754–1760. https://doi.org/10.1093/bioinformatics/btp324.

Love, M.I., Huber, W., Anders, S., 2014. Moderated estimation of fold change and dispersion for RNA-seq data with DESeq2. Genome Biol. 15 (12). https://doi.org/10.1186/s13059-014-0550-8.

Maillard, F., Pflender, S., Heckman, K.A., Chalot, M., Kennedy, P.G., 2022. Fungal necromass presents a high potential for mercury immobilization in soil. Chemosphere 311, 136994. https://doi.org/10.1016/j.chemosphere.2022.136994.

Mazuecos-Aguilera, I., Anta-Fernández, F., Crespo-Barreiro, A., Martínez-Quesada, A., Lombana-Larrea, L., González-Andrés, F., 2025. Plant growth-promoting

rhizobacteria enhanced induced systemic resistance of tomato against *Botrytis cinerea* phytopathogen. Front. Plant Sci. 16. https://doi.org/10.3389/fpls.2025.1570986.
Mei, S., Wang, M., Salles, J.F., Hackl, T., 2023. Diverse rhizosphere-associated *Pseudomonas* genomes isolated along the marine-terrestrial transition zone of a Wadden island salt march. bioRxiv (Cold Spring Harbor Laboratory). 10.1101/2023.11.14.566819.
Meyer, L., Guyot, S., Chalot, M., Capelli, N., 2023. The potential of microorganisms as biomonitoring and bioremediation tools for mercury-contaminated soils. Ecotoxicol. Environ. Saf. 262, 115185. https://doi.org/10.1016/j.ecoenv.2023.115185.
Morales, M., Sentchilo, V., Hadadi, N., Van Der Meer, J.R., 2021. Genome-wide gene expression changes of *Pseudomonas veronii* 1YdBTEX2 during bioaugmentation in polluted soils. Environ. Microbiome 16 (1). https://doi.org/10.1186/s40793-021-00378-x.
Norambuena, J., Wang, Y., Hanson, T., Boyd, J.M., Barkay, T., 2017. Low-molecular-weight thiols and thioredoxins are important players in Hg(II) resistance in *Thermus thermophilus* HB27. Appl. Environ. Microbiol. 84 (2). https://doi.org/10.1128/aem.01931-17.
Pan, S., Li, K., Li, L., Li, M., Shi, L., Liu, Y., Yu, X., 2018. A reaction-based ratiometric fluorescent sensor for the detection of Hg(ii) ions in both cells and bacteria. Chem. Commun. 54 (39), 4955. https://doi.org/10.1039/c8cc01031e, 4958.
Pant, R., Dhyani, N., Arya, P., Tripathy, S., Gupta, A., 2024. Molecular mechanism of mercury -toxicity and tolerance in microbes. In: Earth and environmental sciences library. 159–184. 10.1007/978-3-031-48817-7_7.
Papon, N., Stock, A.M., 2019. Two-component systems. Curr. Biol. 29 (15), R724–R725. https://doi.org/10.1016/j.cub.2019.06.010.
Pramanik, K., Mandal, S., Banerjee, S., Ghosh, A., Maiti, T.K., Mandal, N.C., 2021. Unraveling the heavy metal resistance and biocontrol potential of *Pseudomonas* sp. K32 strain facilitating rice seedling growth under Cd stress. Chemosphere 274, 129819. https://doi.org/10.1016/j.chemosphere.2021.129819.
Prjibelski, A., Antipov, D., Meleshko, D., Lapidus, A., Korobeynikov, A., 2020. Using SPAdes de novo assembler. Curr. Protoc. Bioinform. 70 (1). https://doi.org/10.1002/cpbi.102.
Quintana, J., Novoa-Aponte, L., Argüello, J.M., 2017. Copper homeostasis networks in the bacterium *Pseudomonas aeruginosa*. J. Biol. Chem. 292 (38), 15691–15704. https://doi.org/10.1074/jbc.m117.804492.
Rice, K.M., Walker, E.M., Wu, M., Gillette, C., Blough, E.R., 2014. Environmental mercury and its toxic effects. J. Prev. Med. Public Health 47 (2), 74–83. https://doi.org/10.3961/jpmph.2014.47.2.74.
Schindelin, J., Arganda-Carreras, I., Frise, E., Kaynig, V., Longair, M., Pietzsch, T., Preibisch, S., Rueden, C., Saalfeld, S., Schmid, B., Tinevez, J., White, D.J., Hartenstein, V., Eliceiri, K., Tomancak, P., Cardona, A., 2012. Fiji: an open-source platform for biological-image analysis. Nat. Methods 9 (7), 676–682. https://doi.org/10.1038/nmeth.2019.
Shi, D., Li, D., Zhang, Y., Li, X., Tao, Y., Yan, Z., Ao, Y., 2019. Effects of *Pseudomonas alkylphenolica* KL28 on immobilization of Hg in soil and accumulation of Hg in cultivated plant. Biotechnol. Lett. 41 (11), 1343–1354. https://doi.org/10.1007/s10529-019-02736-9.
Silby, M.W., Winstanley, C., Godfrey, S.A., Levy, S.B., Jackson, R.W., 2011. *Pseudomonas* genomes: diverse and adaptable. FEMS Microbiol. Rev. 35 (4), 652–680. https://doi.org/10.1111/j.1574-6976.2011.00269.x.
Singh, S., Kumar, V., Gupta, P., Ray, M., Kumar, A., 2021. The synergy of mercury biosorption through *Brevundimonas* sp. IITISM22: Kinetics, isotherm, and thermodynamic modeling. J. Hazard. Mater. 415, 125653. https://doi.org/10.1016/j.jhazmat.2021.125653.
Sone, Y., Mochizuki, Y., Koizawa, K., Nakamura, R., Pan-Hou, H., Itoh, T., Kiyono, M., 2013. Mercurial-resistance determinants in *Pseudomonas* strain K-62 plasmid pMR68. AMB Express 3 (1). https://doi.org/10.1186/2191-0855-3-41.
Sperandio, V., Torres, A.G., Kaper, J.B., 2002. Quorum sensing *Escherichia coli* regulators B and C (QseBC): a novel two-component regulatory system involved in the regulation of flagella and motility by quorum sensing in *E. coli*. Mol. Microbiol. 43 (3), 809–821. https://doi.org/10.1046/j.1365-2958.2002.02803.x.
Stratton, A., Ericksen, M., Harris, T.V., Symmonds, N., Silverstein, T.P., 2016. Mercury (II) binds to both of chymotrypsin's histidines, causing inhibition followed by irreversible denaturation/aggregation. Protein Sci. 26 (2), 292–305. https://doi.org/10.1002/pro.3082.
Tambong, J.T., Xu, R., Bromfield, E.S.P., 2016. *Pseudomonas canadensis* sp. nov., a biological control agent isolated from a field plot under long-term mineral fertilization. Int. J. Syst. Evol. Microbiol. 67 (4), 889–895. https://doi.org/10.1099/ijsem.0.001698.
Theodoulou, F.L., Kerr, I.D., 2015. ABC transporter research: going strong 40 years on. Biochem. Soc. Trans. 43 (5), 1033–1040. https://doi.org/10.1042/bst20150139.
Uehara, T., Park, J.T., 2008. Growth of *Escherichia coli*: significance of peptidoglycan degradation during elongation and septation. J. Bacteriol. 190 (11), 3914–3922. https://doi.org/10.1128/jb.00207-08.
Vats, P., Kaur, U.J., Rishi, P., 2022. Heavy metal-induced selection and proliferation of antibiotic resistance: a review. J. Appl. Microbiol. 132 (6), 4058–4076. https://doi.org/10.1111/jam.15492.
Vergnes, A., Henry, C., Grassini, G., Loiseau, L., Hajj, S.E., Denis, Y., Galinier, A., Vertommen, D., Aussel, L., Ezraty, B., 2022. Periplasmic oxidized-protein repair during copper stress in *E. coli*: a focus on the metallochaperone CusF. PLoS Genet. 18 (7), e1010180. https://doi.org/10.1371/journal.pgen.1010180.
Wiatrowski, H.A., Ward, P.M., Barkay, T., 2006. Novel reduction of mercury(II) by mercury-sensitive dissimilatory metal reducing bacteria. Environ. Sci. Technol. 40 (21), 6690–6696. https://doi.org/10.1021/es061046g.
Xiang, Y., Liu, G., Yin, Y., Cai, Y., 2022. Binding characteristics of Hg(II) with extracellular polymeric substances: implications for Hg(II) reactivity within periphyton. Environ. Sci. Pollut. Res. 29 (40), 60459–60471. https://doi.org/10.1007/s11356-022-19875-8.
Xu, J., Bravo, A.G., Lagerkvist, A., Bertilsson, S., Sjöblom, R., Kumpiene, J., 2014. Sources and remediation techniques for mercury contaminated soil. Environ. Int. 74, 42–53. https://doi.org/10.1016/j.envint.2014.09.007.
Zhang, J., Zeng, Y., Liu, B., Deng, X., 2020. MerP/MerT-mediated mechanism: a different approach to mercury resistance and bioaccumulation by marine bacteria. J. Hazard. Mater. 388, 122062. https://doi.org/10.1016/j.jhazmat.2020.122062.
Zhang, S., Yang, G., Jiang, Y., 2022. Antibiotic and metal resistance of *Stenotrophomonas maltophilia* isolates from Eboling permafrost of the Tibetan Plateau. Environ. Sci. Pollut. Res. 30 (5), 11798–11810. https://doi.org/10.1007/s11356-022-22888-y.
Zheng, R., Wu, S., Ma, N., Sun, C., 2018. Genetic and physiological adaptations of marine bacterium *Pseudomonas stutzeri* 273 to mercury stress. Front. Microbiol. 9. https://doi.org/10.3389/fmicb.2018.00682.